IDENTIFYING ICE HYDROMETEOR SIGNATURES ABOVE SUMMIT, GREENLAND USING A MULTI-INSTRUMENT APPROACH

By

CLAIRE PETTERSEN

A thesis submitted in partial fulfillment of

the requirements for the degree of

Master of Science

(Atmospheric and Oceanic Sciences)

at the

UNIVERSITY OF WISCONSIN-MADISON

2014

APPROVED

Advisor Title:

Ralf Bennartz, Ph.D.

University of Wisconsin – Madison

Department of Atmospheric and Oceanic Sciences

_____

Advisor Signature

_____

Date

ABSTRACT

Ground-based microwave radiometers are commonly used to retrieve precipitable water vapor and liquid water path. These retrievals, however, may be adversely affected by ice hydrometeors commonly observed in mixed phase clouds. Research on the effect of ice hydrometeors on the microwave signal is insufficient. We establish that ice hydrometeors produce enhanced brightness temperatures in high frequency ground-based passive microwave observations. This effect is evident in several years of summer season microwave radiometer data collected at Summit Station, Greenland. Using a multi-instrument suite and coupling measurements with well-established gas and liquid absorption models, we can quantify the ice hydrometeor signature. Better knowledge of these ice effects on the passive microwave observations aids in improvement of retrieved properties, such as liquid water path, when ice is present in the column. Additionally, the use of the active cloud radar guides what regimes exhibit predominately ice precipitation. By clearly identifying the ice signature in the high frequency microwave, we have established a standard by which to compare ice habit models and particle size distributions.

ACKNOWLEDGEMENTS

First, I would like to thank my advisor, Professor Ralf Bennartz, who exudes an enthusiasm for atmospheric science that is contagious and whose encouragement was key to my involvement with the Atmospheric and Oceanic Sciences Department and the ICECAPS Project. Researcher Mark Kulie spent many an hour (of which he had few) helping me sort through the details of the radiative transfer and ice models. Mark radiates excitement for our field of study that is energizing and helped me keep on trying new avenues when it felt like all possibilities were exhausted. Co-Principal Investigators with the ICECAPS Project, Dave Turner and Matt Shupe, lent their expertise to many instruments and retrievals and science related to this project and both had excellent suggestions for further research and related topics. Professor Grant Petty aided me with questions about the ice habits and scattering properties and is excited to continue to collaborate on further ice-related studies. Professor Tristan L'Ecuyer is not only a close friend, but also an excellent sounding board over a beer with limitless excitement about and ideas for this and future work. I am super fortunate to have a best friend and partner who works in the same field of study: Researcher Aronne Merrelli and I spend many a meal, beer, walk, etc. chatting about atmospheric science including a lot related to this research and whose help without which this research would not have been possible. Finally, my supervisor Fred Best (Associate Director of Technology at SSEC) has not only been supportive, but actively interested in the evolution of this work and has encouraged me to pursue scientific questions which are of interest me, even if they are not directly related to his projects.

TABLE OF CONTENTS

1. Introduction

Quantifying the effect of ice hydrometeors on microwave radiation in the atmosphere is a non-trivial task, even with modern high-resolution active and passive instruments. Ice hydrometeors change the path and net effect of downwelling radiation, but isolating the signature of the ice is challenging. In many cases the signature is small relative to the signatures of liquid water and gas absorption. Additionally, the ice hydrometeor signal can interfere with retrievals of other atmospheric properties. By better understanding ice hydrometeor characteristics, we can separate their effect and improve atmospheric retrievals based on microwave remote sensing instruments. In turn, this will improve the derived climatologies of cloud properties from microwave remote sensing, especially from ground-based sensors. To address these topics, this study will focus on observations from an instrument suite located in the Arctic on the Greenland ice cap, as it is a unique and isolated environment in which to observe ice hydrometeor characteristics.

1.1 Arctic Importance

The Greenland Ice Sheet (GIS) is of particular interest as it has relatively large impacts on the Earth's climate system (Church *et al.*, 2001). Understanding the characteristics of precipitation above the GIS is a key factor in quantifying the full radiation and ice mass balance. The site of the Greenland Ice Sheet Project 2 (GISP2) ice core project has expanded to a continuously operational science facility, Summit Station, dedicated to studying the atmosphere and ice sheet properties of the GIS (see Figure 1.1), which has been key to temperature and chemical dating throughout Earth's history as well as understanding

climate processes (Dansgaard *et al.*, 1993). Summit Station is home to many atmospheric and snow science instruments, including the Integrated Characterization of Energy, Clouds, Atmospheric State, and Precipitation at Summit (ICECAPS; Shupe *et al.*, 2013) suite purposely co-located at Summit Station to continue to aid in understanding how the GIS cryosphere and atmosphere change over time. Since 2010, the ICECAPS suite of instruments has been monitoring a variety of atmospheric parameters to further our knowledge of atmospheric processes above the GIS (Shupe *et al.*, 2013). The ICECAPS project will remain at Summit until at least 2018, thus providing a comprehensive dataset and analyses of the atmosphere over central Greenland and expanding the network of past and existing high-latitude atmospheric suites (i.e., Eureka, Canada and Barrow, Alaska) already helping to characterize Arctic atmospheric processes (Shupe *et al.*, 2011).

1.2 Enhanced Downwelling Radiance in the Presence of Ice

A commonly implemented technique for characterizing ice hydrometers from satellites is to use high-frequency channels (89GHz and greater) in passive microwave instruments and look for depressed brightness temperatures (Hong *et al.*, 2005; Kulie *et al.*, 2010). This technique is based on the idea that while liquid and gas in the atmospheric column will emit a relatively warm brightness temperature, the ice hydrometeors will scatter surface emission away from the satellite sensor and therefore depress the brightness temperature artificially. The same technique can be used from the ground looking up, however, with the opposite effect. Kneifel *et al.* (2010) demonstrated the presence of a signature from ice hydrometeors for a case study of snowfall in the Alps using ground-based microwave radiometers (MWRs). The high-frequency MWR, 90 and 150 GHz, channels are

"window channels" that see through the atmosphere nearly unimpeded to space; however, when ice or liquid water is present these channels see a higher brightness temperature (see Figure 1.2).

Consequently, if there are ice hydrometeors present, they will have two effects on the observed brightness temperatures: emission of radiation and scattering some of the surface radiation back at the instrument. These two effects will thus enhance the measured brightness temperature compared to a column with no ice. Since some of the ice signature is the scattered surface radiation, it is related to both the surface temperature and emissivity. Therefore, this makes the ice signature challenging to model because it depends on both properties of the ice hydrometeors and the surface.

In general, the ice hydrometeors will have fairly high single scatter albedo (SSA) at high microwave frequencies, regardless of habit and size distribution (see Figure 1.3), and will therefore scatter some of the surface radiation back to the instrument. The surface emissivity of different types of snow seen at Summit varies in the range of 0.60 to 0.91 for the higher frequency passive microwave channels used in this study (Yan, 2008). Additionally, the ice will have some emission, which will increase the brightness temperature a small amount. Due to the combination of these two effects – the scattering of radiation back to the surface and the slight emission from the ice hydrometeors – the measurements from ground-based high frequency MWRs will exhibit an enhanced brightness temperature. We propose that by combining the observed data from instruments in the ICECAPS suite with radiative transfer models of the gas and liquid in the atmosphere, this enhanced brightness temperature from the ice hydrometeors can be isolated and quantified. Because the ice signature is also dependent on ice crystal habit and size distribution, relying on a

small number of precipitation events to derive the ice signature may bias the result toward specific precipitation situations. The large dataset from the ICECAPS Project allows for the average ice signature to be computed over many precipitation events, thus reducing this potential sampling bias.

1.4 Figures

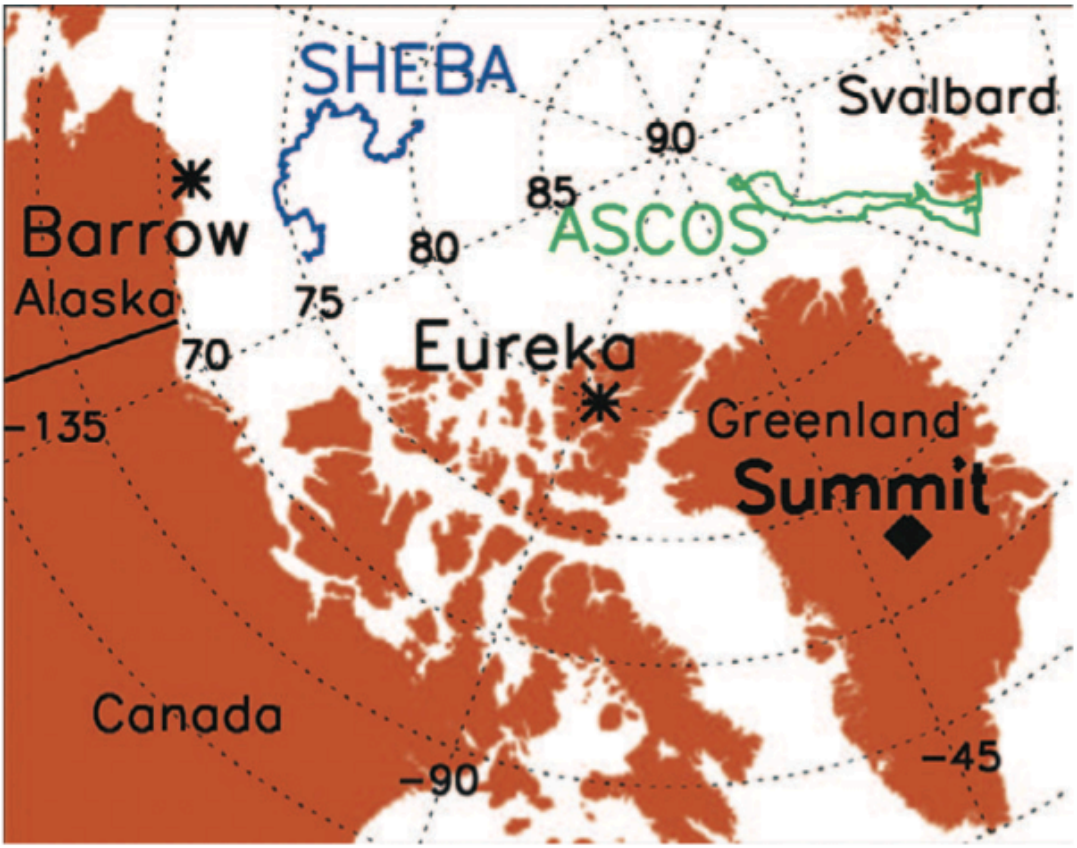

Figure 1.1: Location of ICECAPS Suite at Summit Station, Greenland *(Figure 1. from Shupe et al., 2013).*

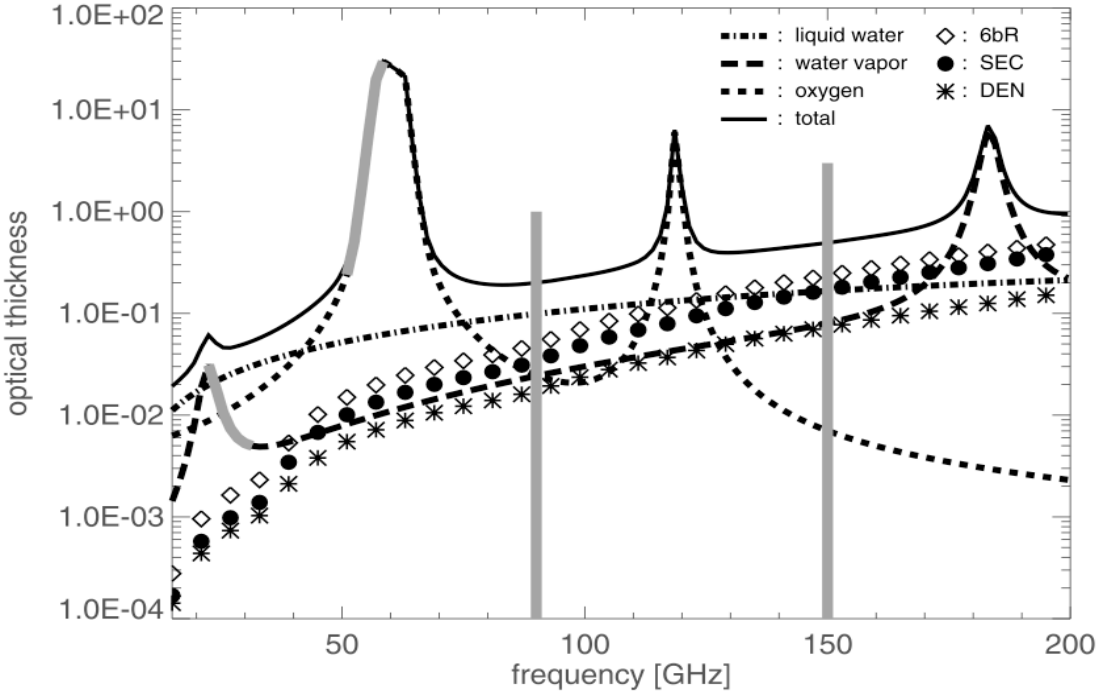

Figure 1.2: Model results of optical thickness as a function of frequency from Kneifel *et al.*, for atmospheric conditions on 8 February 2009. Microwave radiometer channels for the ranges measured are show in the gray boxes. *(Figure 2 from Kneifel et al., 2010).*

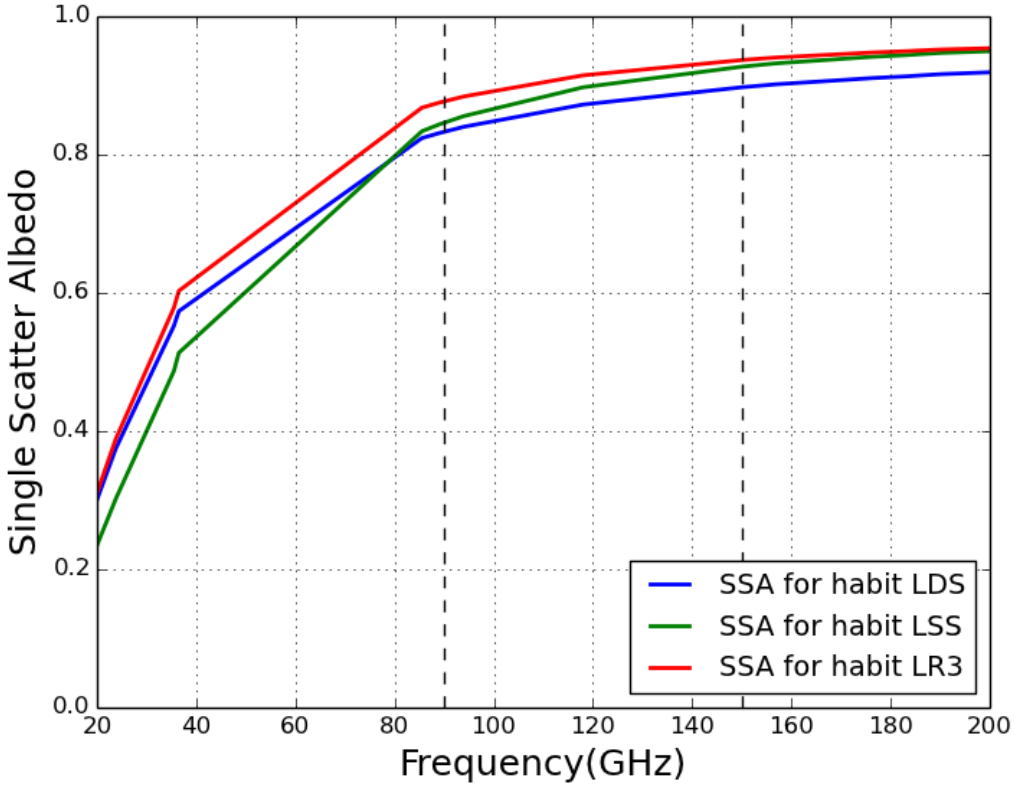

Figure 1.3: Single scatter albedo (SSA) of different ice habits as a function of frequency. Assumed a snow water content (SWC) of 0.1m/g^3, a temperature of -20°C, and a particle size distribution from Field *et al.* (2007) to calculate the optical properties. The dashed lines indicated the high frequency channels – 90 and 150 GHz. Though the SSA values are large at high frequency and therefore are scattering much of the radiation back to the instruments, we still must consider emission from the snow as part of the enhanced brightness temperatures observed by the MWRs.

2. Datasets and Methods

Studying the seasonal characteristics of the ice hydrometeors above the GIS is made possible from observations from the ICECAPS instrument suite from 2010 to 2013. In addition, modeling the atmospheric column using common gas and liquid radiative transfer models can add information when combined or compared with observations from specific instruments in the ICECAPS suite. We will first illustrate the instruments and their respective measurement and retrieval capabilities (Section 2.1). Next, we will describe the radiative transfer models used in this study (Section 2.2).

2.1 ICECAPS Project and Instrument Suite

The ICECAPS instrument suite located at Summit Station, Greenland, in operation since October 2010 (through at least October, 2018), is part of the United States Arctic Observation Network (US AON). ICECAPS is modeled after other successful Arctic observatories (see Figure1.1) and is similar in scope to facilities run by the Department of Energy's Atmospheric Radiation Measurement (ARM) Program (Ackerman *et al.*, 2003). The ICECAPS instrument suite is supported by a seasonal technician as well as the support staff at Summit Station and is updated with new instruments, upgrades, and repairs by researchers every summer. Table 2.1 illustrates a brief overview of all the ICECAPS instruments, including the key specifications, measurements, and retrieved parameters. For this study, we employed data from a subgroup of the available measurements and retrieved values described in the following sections.

2.1.1 Millimeter Cloud Radar

The Millimeter Cloud Radar (MMCR) is a zenith pointing, 35GHz (Ka band) radar with measurements taken every two seconds with a height resolution of 45 meters (see top, center of Figure 2.1; Moran *et al.*, 1998). The MMCR measures the reflectivity, Doppler velocities, and Doppler spectral width of the hydrometeors in the column above. For the 35 GHz MMCR, hydrometeors with geometric diameters less than or approximately 3 mm are in the Rayleigh region (Kneifel *et al*., 2011). Therefore the backscatter cross-section of these small ice hydrometeors is proportional to diameter to the sixth power (Reinhart, 2010):

$$\sigma = \frac{\pi^5 |K|^2 D^6}{\lambda^4}$$

And the radar power is a function of the backscattering cross-section:

$$p_r = \frac{p_t g^2 \lambda^2 \sigma}{64\pi^3 r^4}$$

Where *r* is the range from the radar and the others in the equation are constants defined by the type of radar. Consequently, the power measured by the MMCR is proportional to the diameter of the hydrometeor raised to the sixth power for the hydrometeors in the Rayleigh region. However, for ice hydrometeors larger than ~3 mm diameter the Rayleigh approximation breaks down (at this size, the MMCR starts to see Mie resonance effects) and the backscatter cross-section depends on ice habit (Kneifel *et al.*, 2011; Petty and Huang, 2010).

The speed of the hydrometeors falling towards the MMCR can be measured using the Doppler effect: shifting of the frequency, which is proportional to direction and velocity of the object traveling. Since the fall speed of a hydrometeor is much less than that of the speed of light, the velocity can be approximated as:

$$V \approx \frac{f_d \lambda}{2}$$

Where f_d is the frequency shift created by the falling hydrometeor and λ is the wavelength of the radar. The Doppler velocity measures the fall speed (or perceived fall speed) of the particle – this is dependent on the mass and projected area of the ice hydrometer, thus some microphysical insight is gained from these fall speed values. However, the various up/downdrafts and eddies experienced by the particle will effect the fall speed.

Finally, the variance of the velocity, the Doppler spectral width, aids in determining turbulence and occurrence of like hydrometeors. For example: when there is a lot of turbulence in a cloud layer, the Doppler spectral width observed is high; when snow hydrometeors of similar shape – thus similar fall speed – are precipitating out of a cloud, the Doppler spectral width is low. By combining these measurable quantities from the MMCR, we can characterize the properties of the large hydrometeors observed at Summit.

2.1.2 Microwave Radiometers

In addition to the active microwave instrument, the MMCR, ICECAPS also uses observations from passive Microwave Radiometers (MWRs). There are two different MWRs used in this study: the Humidity and Temperature Profiler (HATPRO) and a high-frequency passive microwave instrument (MWRHF) built by Radiometer Physics GmbH (see top, left of Figure 2.1). The HATPRO has seven channels from 22-32GHz and seven channels from 51-58GHz and the MWRHF has two high-frequency channels: 90 and 150GHz, which take measurements every four seconds (Rose *et al.*, 2005). Both MWRs measure the downwelling brightness temperature of the atmospheric column in their respective channels' frequencies for a given zenith angle.

Passive microwave radiometry is commonly used to derive liquid water path (LWP) to a fairly accurate degree (Crewell *et al.*, 2008). By combining the brightness temperatures observed from specific channels (23.84, 31.40, 90, and 150GHz), a column precipitable water vapor (PWV) and LWP are derived using the MWR Retrieval (MWRRET) algorithm (Turner *et al.*, 2007). The addition of the high frequency channels to the retrieval algorithm for the LWP creates more accuracy – better than 12 g/m^2 (Crewell *et al.*, 2008), which is important as cloud liquid water on average at Summit (and the Arctic as a whole) is very small. In fact, 80% of liquid-bearing clouds in the Arctic have less than $100g/m^2$ LWP (Turner *et al.*, 2007a) and, as we will show in Section 3, Summit Station has even smaller amounts of LWP in the liquid-bearing clouds observed in this study.

2.1.3 Ceilometer

The microwave retrieval gives the integrated path of the cloud liquid water but no information about cloud altitude. Cloud base height (CBH) is estimated from a Vaisala Ceilometer (VCEIL), shown top, center in Figure 2.1. The VCEIL has a vertically pointing 905 nm laser with 15 meter height resolution and takes a measurement every 15 seconds. Based on the backscattered signal received by the instrument, cloud base heights (up to three layers) are determined. In this work, the first cloud base height retrieved from the VCEIL is used to define the liquid water layer.

2.1.4 Radiosondes

Data from twice daily balloon radiosondes (manufactured by Vaisala) launched at Summit Camp near the ICECAPS instrument suite (within 50 meters) at approximately 1200 and 2400 Coordinated Universal Time (UTC) are also utilized in this study. The radiosonde launches gather measurements of the temperature, pressure, relative humidity, and, in some

cases, the horizontal wind speeds and directions. For this work, the temperature, pressure, and relative humidity are included in the analysis.

2.2 Radiative Transfer Model for Gas and Liquid

The emission and absorption of the gases and liquid water in the atmospheric column are modeled using *in situ* observations of temperature and pressure and remotely sensed values of scaled water vapor, liquid water content, and cloud base height from the ICECAPS instruments, illustrated in Figure 2.2. To compute the volume absorption coefficients of dry air and water vapor in the atmospheric column, we employed the Rosenkranz Model (Rosenkranz, 1998) using inputs of layer temperature, pressure, and water vapor (see Figure 2.3, green and blue lines, respectively). The liquid water absorption and emission is modeled using the Liebe Model (Liebe *et al.*, 1991) with inputs of liquid water content (LWC) at a defined cloud height (see Figure 2.3, red line).

For an example day, we would use data from the prior day's radiosonde launch (day -1, 2400 UTC) along with the two radiosondes launched for the given day (1200 and 2400 UTC) and interpolate the temperature, pressure, and relative humidity of each layer in the column throughout the day to the MMCR's temporal and vertical grid. Next, the MWR retrieved PWV is used to scale the interpolated relative humidity from the radiosonde – this is because the PWV retrieved value is higher temporal resolution and more accurate than the radiosonde data (Turner *et al.*, 2000). Finally, the MWR retrieved LWP values are converted into a liquid water content (LWC, units of g/m^3) and placed in a single layer in the column with height defined by the first cloud base height (CBH1) detected by the VCEIL. All the

inputs are run in the gas, Rosenkranz, and liquid, Liebe, absorption/emission models and output as volume absorption coefficients per atmospheric layer at a desired frequency.

2.3 Successive Order of Interaction Radiative Transfer Model

Once ice hydrometeors are introduced into the atmosphere there is now the possibility of multiple scattering, therefore we must employ an additional radiative transfer model to attempt to simulate the effects of ice. The Successive Order of Interaction (SOI) radiative transfer model accounts for multiple scattering (Heidinger *et al.*, 2006). For the case of the microwave channels we use in this study, the SOI model is typically better than 1K for precipitation (O'Dell *et al.*, 2006). The SOI model combines the layered averaged optical properties and temperature in order compute downwelling radiance at selected frequencies. The layered averaged optical properties are calculated from the gas and liquid water models (described above) and ice optical properties (further discussed in Section 5). The SOI modeled brightness temperatures can then be compared to MWR observations (see Figure 2.2). For all cases used in this study we employed the SOI radiative transfer model, even when modeling non-scattering atmospheres that only include the gas and liquid absorption. As is further discussed in the subsequent section, comparing the measured and modeled brightness temperatures at specific frequencies lends insight into the hydrometers present in the atmospheric column.

2.3 Tables and Figures

TABLE 1. ICECAPS instrument specifications, measurements, and derived parameters. All instruments other than the IcePIC and radiosondes are pointed approximately in the zenith direction. Instrument resolutions are given as "res."

Instrument name	Key specifications	Primary measurements	Derived parameters	Institution
P-AERI	530–3,000 cm^{-1} (3–19 μm), 1 cm^{-1} res., <1-min time res.	Downwelling spectral infrared radiance	Cloud phase and microphysics, atmospheric temperature	University of Idaho
MWRHF	Frequencies: 90, 150 GHz, 2–4-s time res.	Downwelling brightness temperatures	Cloud LWP, PWV	University of Wisconsin
HATPRO	Frequencies: 7 channels 22–32 GHz, 7 channels 51–58 GHz, 2–4-s time res.	Downwelling brightness temperatures	Cloud LWP, PWV, atmospheric temperature	University of Wisconsin
MMCR	Ka band (35 GHz), 8-mm wavelength, 2-s time res., 45-m vertical res.	Reflectivity, mean Doppler velocity, Doppler spectrum width, Doppler spectra	Cloud boundaries, phase, microphysics; cloud-scale dynamics	NOAA Earth System Research Laboratory (ESRL)
MPL	532-nm wavelength, 5-s time res., 15-m vertical res., 2°–4° off zenith	Relative backscatter, hybrid linear–circular depolarization ratio	Cloud-base height, phase, microphysics	DOE ARM
CAPABL	523-nm wavelength, 15-s time res., 30-m vertical res., three-channel receiver, 2°–11° off zenith	Backscatter, linear depolarization ratio, diattenuation	Cloud-base height, phase, microphysics	NOAA/ESRL
Ceilometer	905-nm wavelength, 15-m vertical res., 15-s time res.	Backscatter	Cloud-base height	DOE ARM
POSS	X-band (10.5 GHz), 1-min time res., single volume near surface	Reflectivity, Doppler spectra	Precipitation rate	Environment Canada
Sodar	2,100 Hz, <1-m vertical res., 1-s time res.	Reflectivity	Boundary layer depth	NOAA/ESRL
IcePIC	Canon D50 DSLR, ~5.6 magnification, 1.5 μm res., 6.1 megapixels	Digital photographs	Ice crystal habit	University of Idaho
Radiosondes	1-s time res., twice daily, RS-92K or RS-92SGP sondes	Temperature, relative humidity, pressure, winds	Cloud temperature, tropospheric thermodynamic structure	University of Idaho and University of Colorado

Table 2.1: Instrument specifications and their respective measurements for the ICECAPS suite in Summit, Greenland. Instruments used in this study are highlighted in red *(Modified Table 1 from Shupe et al., 2013)*

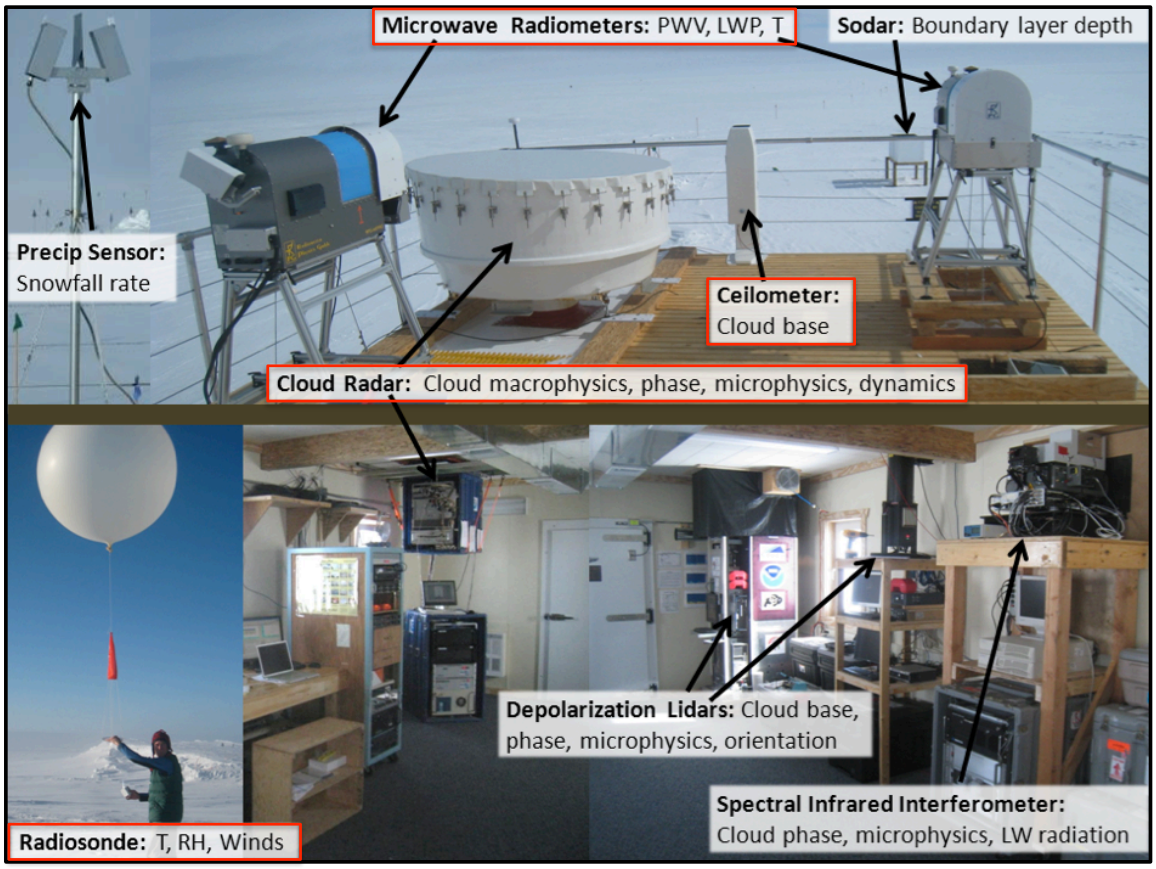

Figure 2.1: Layout of the ICECAPS instrumentation at the Mobile Science Facility at Summit Station. Instruments used in the study are highlighted in red: the Microwave Radiometers, Cloud Radar, ceilometer, and balloon launched radiosondes. *(Modified Figure 2 from Shupe et al., 2013)*

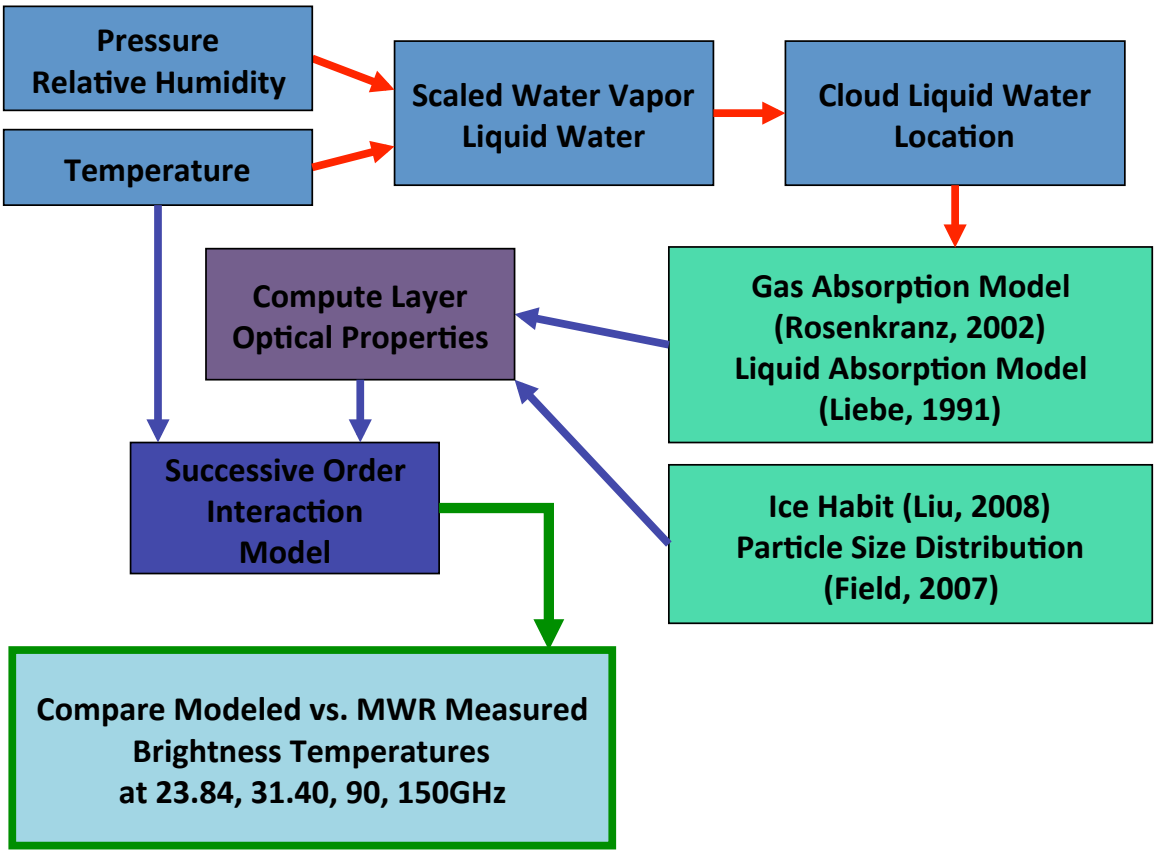

Figure 2.2: Outline of the radiative transfer model with inputs shown in the blue boxes: temperature, pressure, relative humidity from the radiosonde; scaled water vapor and liquid water from the MWR retrieval; cloud liquid water height from the VCEIL. These inputs are run through the radiative transfer models (green box) for gas (Rosenkranz) and liquid (Liebe) absorption and emission. The output volume absorption coefficients are combined with ice habit and particle size distribution to compute the layer optical properties (purple box), which are then combined with the temperature profile and input into the SOI model. Output brightness temperature calculated by the SOI is a function of frequency and can then be compared to the measured values at the same frequencies (teal box).

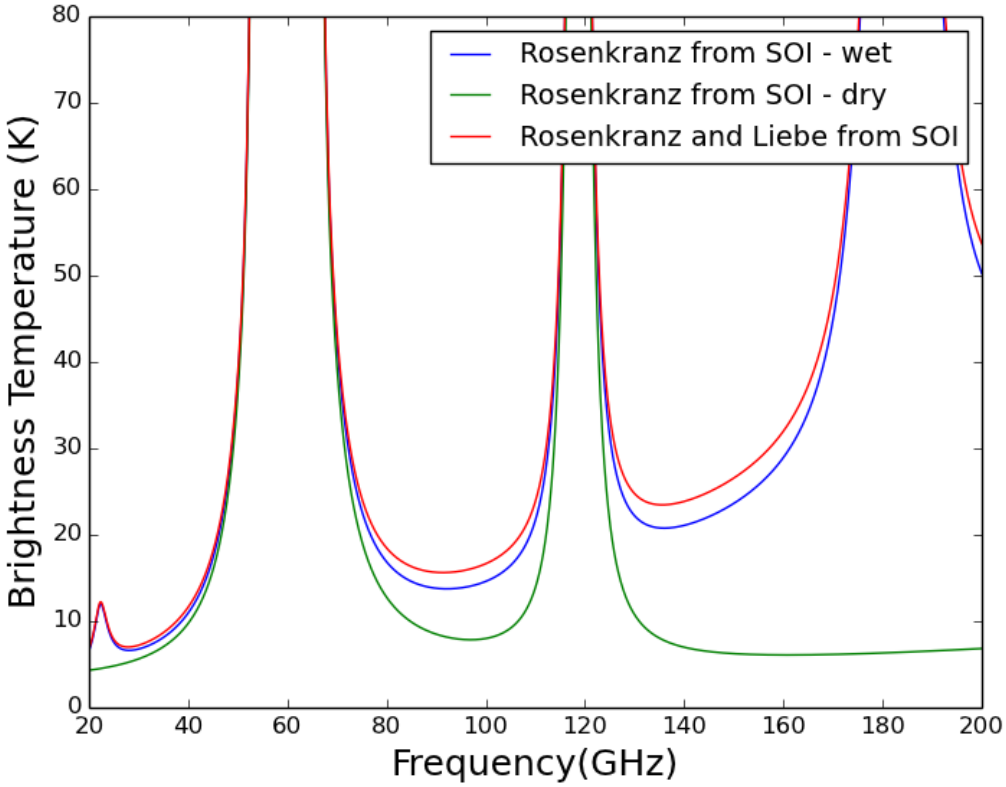

Figure 2.3: Example of the downwelling radiance as a function of frequency for the gas absorption radiative transfer model for the June 30, 2012 2400Z radiosonde. The "wet" case is with a PWV value observed by the 2400Z radiosonde (blue), while the "dry" case is with a PWV value of 0 (green). The downwelling radiance as a function of frequency for the liquid and gas absorption is shown in red.

3. Ice Hydrometeor Behavior as Observed by ICECAPS

Similar to Kneifel *et al.* (2010), we compared the brightness temperatures in the high frequency channels of the MWRs to a modeled output. Kneifel *et al.* (2010) employed both a radiative transfer and a scattering model to simulate the behavior of the ice signature based on the habit, surface emissivity, etc. Different from Kneifel *et al.* (2010), we do not include an ice scattering model for the purpose of identifying the ice signature. We instead attempt to isolate the ice radiative signature in the observations by carefully accounting for any other potential emission or absorption sources within the column. If the calculated brightness temperature using only gas and liquid water is compared to the observed brightness temperatures from the MWRHF, any difference should be due to the ice signature. Consequently, the average ice hydrometeor radiative signature can be computed over many precipitation events by extending the analysis to the full available ICECAPS dataset.

3.1 Characterization of Ice Precipitation at Summit

Merging all available data for the MMCR and plotting a contoured frequency by altitude diagram (CFAD) gives insight into precipitation behavior at Summit. CFADs depict all data as individual points in time, height, and radar measured value (for example, reflectivity) as a two dimensional histogram. Figure 3.1a is a CFAD of all the reflectivity values measured by the MMCR for any given time within the summer months – June, July, August, (JJA) – 2011 through 2013, where the horizontal axis is the reflectivity values and the vertical axis is height and the contours are the frequency of occurrence. By filtering the MMCR reflectivity CFAD, illustrated in Figure 3.1a, as a function of other ICECAPS

instrument measurements or derived parameters; one can highlight the types of hydrometeors observed during specific atmospheric conditions.

Filtering the MMCR CFADs by corresponding MWR-derived LWP for the same summer period for 2010 through 2013 highlights the regimes in which ice hydrometeors are present. As depicted in Figure 3.1b and 3.1c, the MMCR reflectivity CFAD for JJA has been filtered by cases when LWP was less than and greater than 40 g/m^2, respectively. The resulting CFADs are very different from each other and lend insight to the behaviors and phases of the hydrometeors in each case. For the case of less than 40 g/m^2 LWP, the CFAD illustrated common ice hydrometeor behaviors: reflectivity increasing due to ice particle growth, a peak reflectivity of ~0 dBZ, and reflectivity occurrence maximum clearly above the surface (see Figure 3.1b). In contrast, the reflectivity CFAD for the case of LWP greater than 40 g/m^2 has little indication of growth and a maximum of occurrence at a low reflectivity value (around -20 dBZ) at the surface, consequently, little to no indication of significant ice hydrometeors. Additionally, Figure 3.2 depicts all the measurement types from the MMCR as CFADs for less than 40g/m^2 LWP: reflectivity (3.2a), Doppler velocity (3.2b), and Doppler spectral width (3.2c). The addition of the Doppler velocity and spectral width CFADs confirm the signal is dominated by ice hydrometers with relatively high fall speeds and narrow spectral widths (whereas cloud liquid water droplets will have low fall speeds on average).

As shown in the filtered CFADS, the frequency of cases in JJA where the LWP is greater than 40 g/m^2 is ~22%, while the cases where LWP is less than 40g/m^2 is ~63% of the time, and clear sky is the remaining 15% of cases. To maximize the likelihood of seeing ice, we limit our work to focus on cases in JJA with LWP of less than 40 g/m^2, not including the

clear sky. Since cases with LWP of less than 40 g/m^2 represent the majority at Summit during the summer months, we can use this filter to get an accurate characterization of ice hydrometeor behavior while limiting noise from higher liquid water cloud concentration.

3.2 Enhanced Brightness Temperatures at 150GHz

As postulated from previous case studies by Kneifel *et al.* (2010), the higher frequency channels in the ground-based zenith-pointing MWRs will see an enhanced brightness temperature in the presence of ice in the column. Thus, we initially looked at the difference between the measured brightness temperatures from the MWRHF 150GHz channel and the SOI model outputs (with no ice included, gas and liquid contributions only) at that same frequency. As illustrated in the contour plot of the JJA comparison in Figure 3.3, there is a clear increase in the difference of the measured brightness temperatures minus the RT modeled brightness temperatures as a function of the MMCR reflectivity converted to what we refer to as "Z Path" – the column integrated reflectivities with units of mm^6/m^2:

$$Z\ Path = \int 10^{0.1*dBZ}\, dz$$

This MMCR Z Path measurement is related to the amount of backscatter coefficient in the atmospheric column. The use of Z Path is advantageous because it acts as a proxy for ice water path (IWP) that does not rely on conversions that are sensitive to ice habit (Kulie *et al.*, 2010). The brightness temperature differences in the 150 GHz have a clear positive dependence on this value. We argue that the Z Path is directly correlated to ice backscatter and cannot be from liquid, as Summit is never above freezing and thus large liquid hydrometeors are highly unlikely to occur (Pruppacher and Klett, 2000). Therefore, the relationship between the brightness temperature differences at 150 GHz and the MMCR Z

Path indicate that the enhanced brightness temperature signature is caused by ice hydrometeors.

3.3 Depressed Brightness Temperatures in Other Channels

Based on previous studies, we expect to observe this enhanced brightness temperature at the 90GHz as well – a similar but smaller effect compared to the 150GHz brightness temperature differences. The lower frequency channels (23.84 and 31.40GHz) should exhibit no effect from the presence of ice hydrometeors in the column, thus we expect the histogram contours to be nearly vertical for the relationship between the brightness temperature differences and the integrated reflectivity (Z Path). However, as seen in Figure 3.4, all the other frequencies, 23.84 (3.4a), 31.40 (3.4b), and 90 GHz (3.4c), show a clear negative dependence on the integrated reflectivity – therefore indicating that ice hydrometeors are depressing the brightness temperatures seen in these frequencies. Since it is unlikely for the low frequency channels to see a contribution from ice in the column, there must be an issue with the input values to the radiative transfer model (Kneifel *et al.*, 2010).

To confirm this negative dependence was not based on implementation error in our gas and liquid absorption model runs, the same comparison of brightness temperatures was made between the measured values from the MWRs and the calculated brightness temperatures from the Monochromatic Radiative Transfer Model (MonoRTM) used as part of the MWRRET algorithm (Turner *et al.*, 2007). The MonoRTM results (Figure 3.5) show a similar Z Path dependency as the SOI results (Figure 3.4) – positive in the 150 GHz and negative in the other channels. There is a clear sky bias in the SOI modeled brightness temperatures, of about 0.5 – 2 K (low to high frequency channels, respectively) at low Z Path

values. We believe this clear sky bias is due to confirmed differences in the gas absorption models (Rosenkranz versus MonoRTM). Since the SOI and MonoRTM brightness temperatures have a similar Z Path dependence, the clear sky bias does not affect the results with respect to the ice signature.

Two of the inputs for the radiative transfer model are retrieved values based on brightness temperatures from the MWRs: the PWV and LWP. The retrieved PWV will not be significantly affected by the presence of ice hydrometeors, however the retrieval for the LWP employs a four-channel algorithm, which includes the 90 and 150GHz frequencies (Turner *et al.*, 2007). If these high frequency channels have enhanced brightness temperatures when ice is present, this will affect the values of the retrieved liquid water. More precisely, the retrieval will tend to increase the LWP in order to account for the enhanced brightness temperature from the ice hydrometeors, leading to an overestimate of LWP.

3.5 Figures

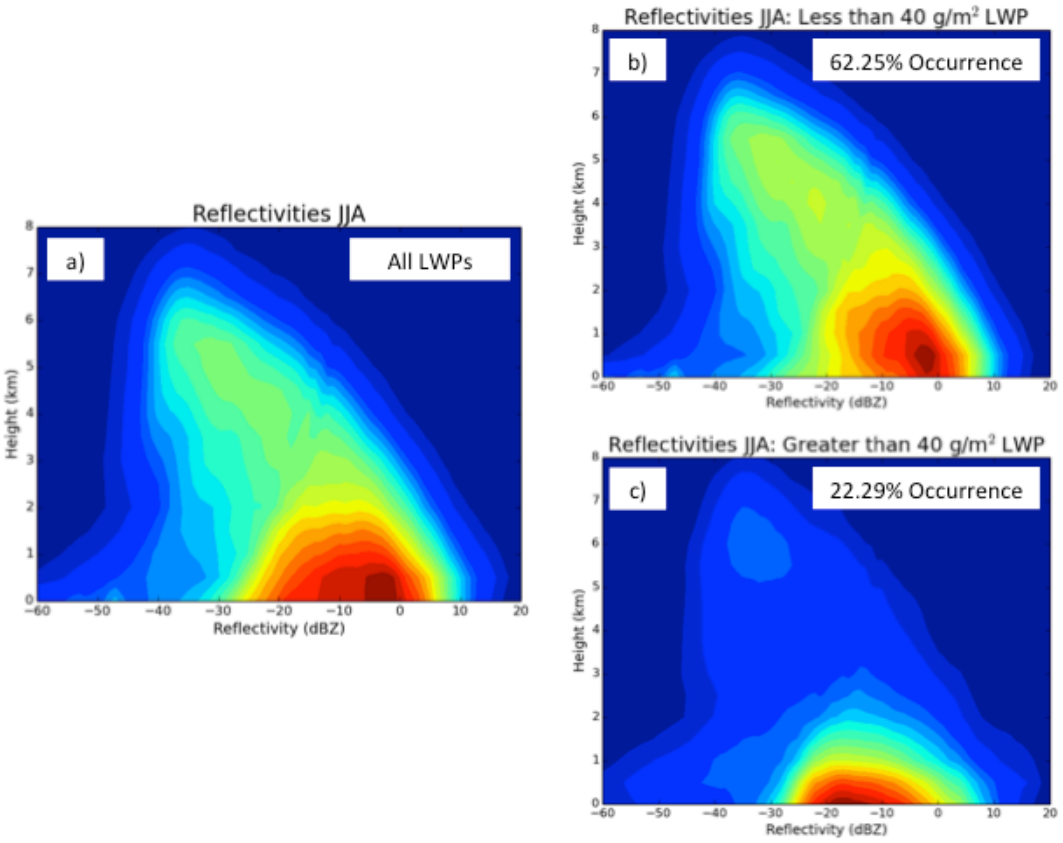

Figure 3.1: CFADs of MMCR reflectivity for summer (JJA) at Summit, Greenland from June 2011 through August 2013. Panel a) shows JJA reflectivity for all measured LWPs while Panel b) is filtered to show CFADs only when LWP is less than 40g/m^2 and Panel c) is filtered for cases greater than 40g/m^2.

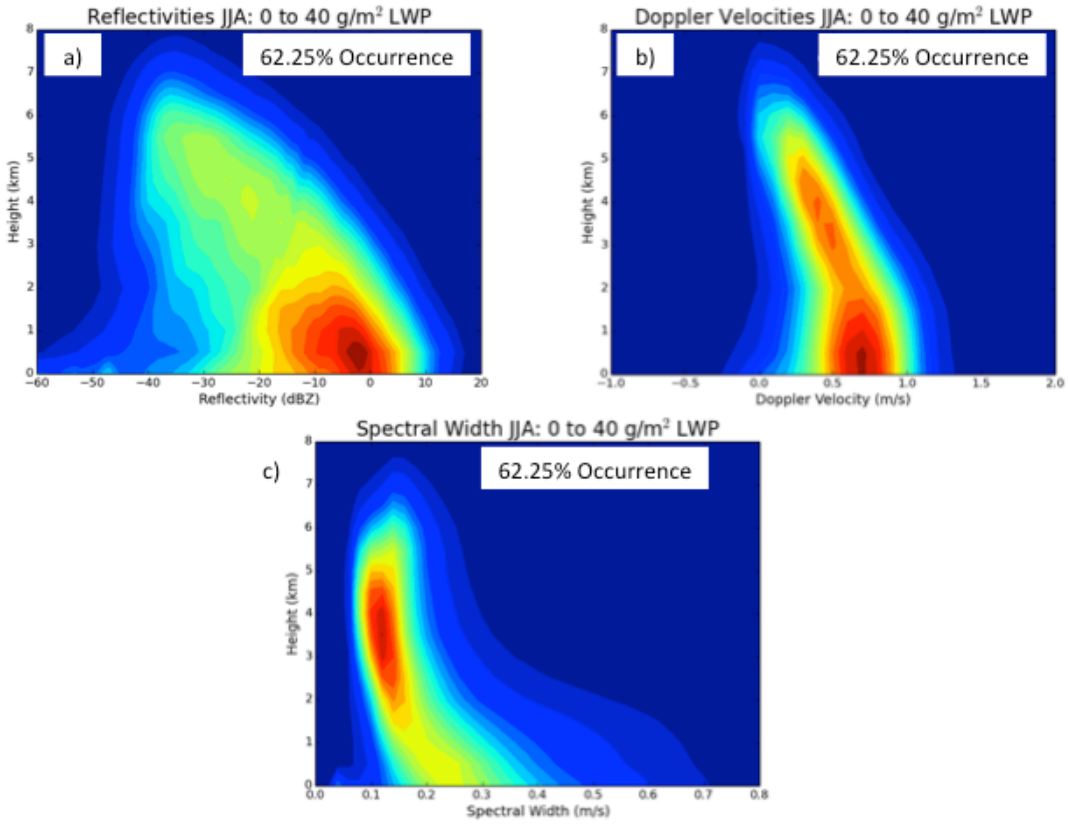

Figure 3.2: CFADs of MMCR properties for summer (JJA) at Summit, Greenland when LWP is less than 40g/m^2. Panel a) shows reflectivities indicative of ice. Panel b) are the Doppler velocities and Panel c) shows the Doppler spectral widths.

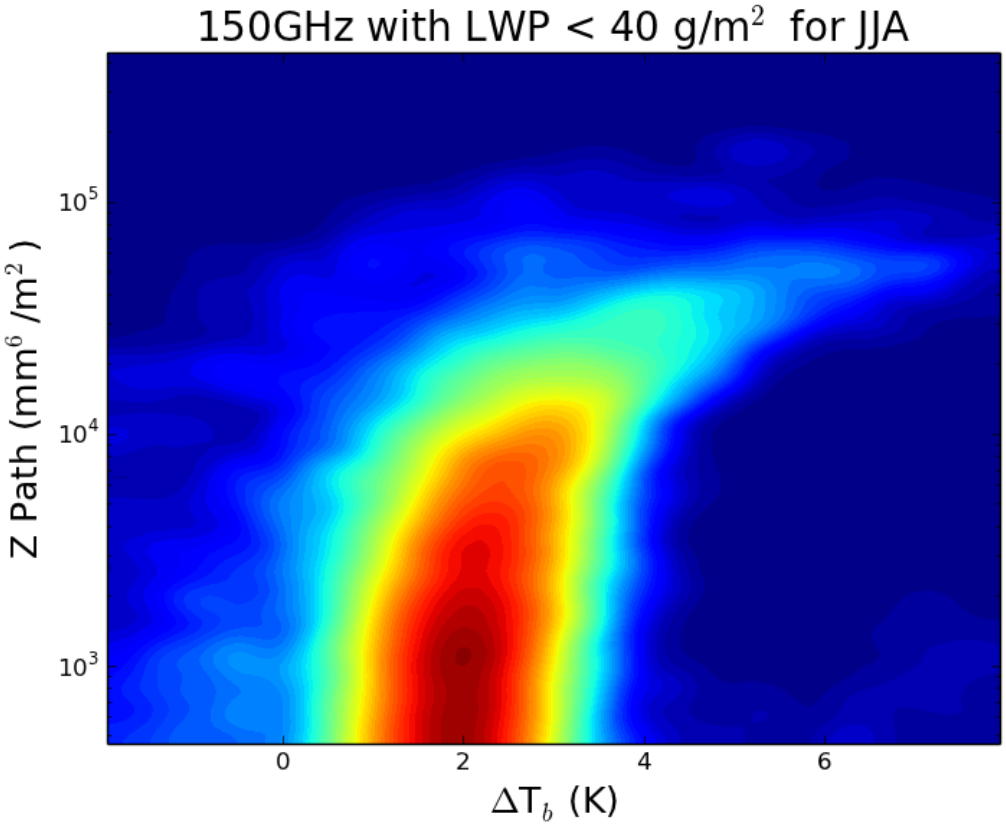

Figure 3.3: Brightness temperature difference between the MWRHF 150GHz channel measurements and the gas and liquid radiative transfer modeled outputs for the summer months (JJA) of June 2011 through August 2013. There is a clear positive dependence of the difference of the calculated from the measured brightness temperature as a function of the Z Path from the MMCR, thus, showing the enhanced brightness temperature as a function of the amount of ice present in the column.

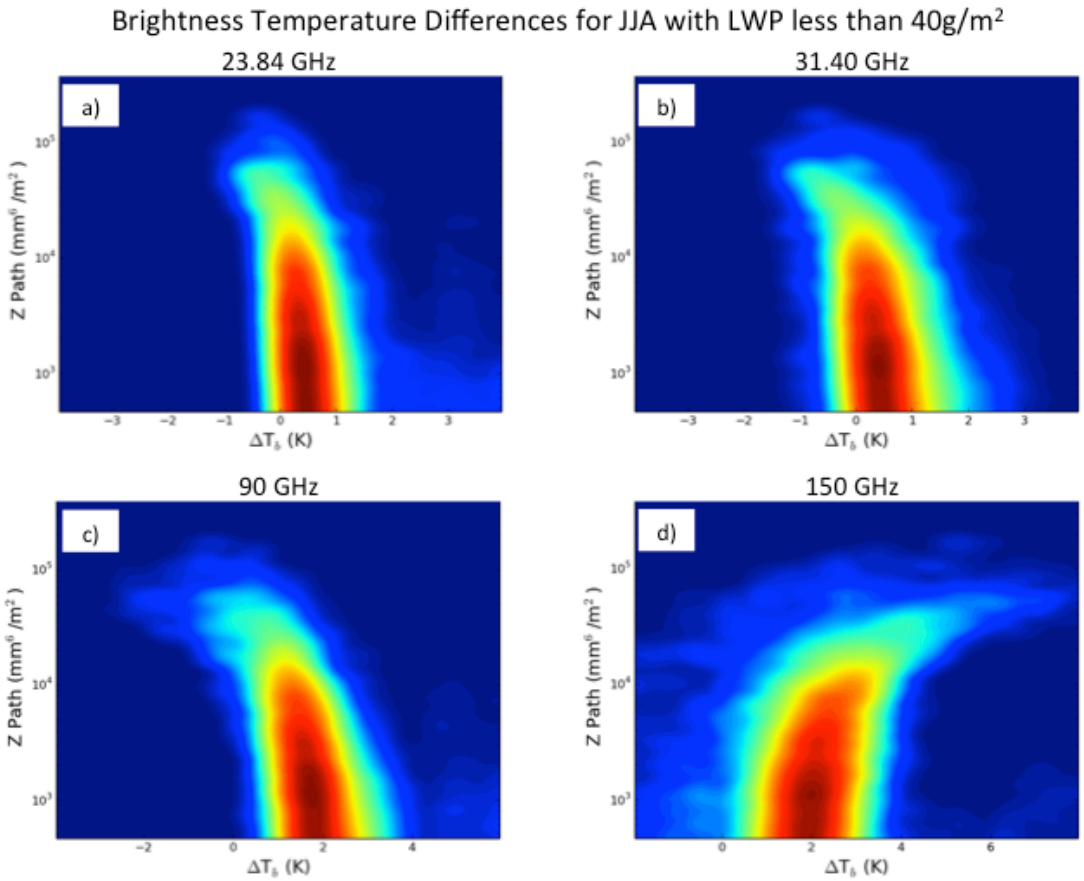

Figure 3.4: Brightness temperature differences between the observations from the MWR and the radiative transfer model for the 23.84, 31.40, 90, and 150GHz channels. The 150 GHz shows enhanced brightness temperatures in the presence of ice; however, the other three channels all show the opposite.

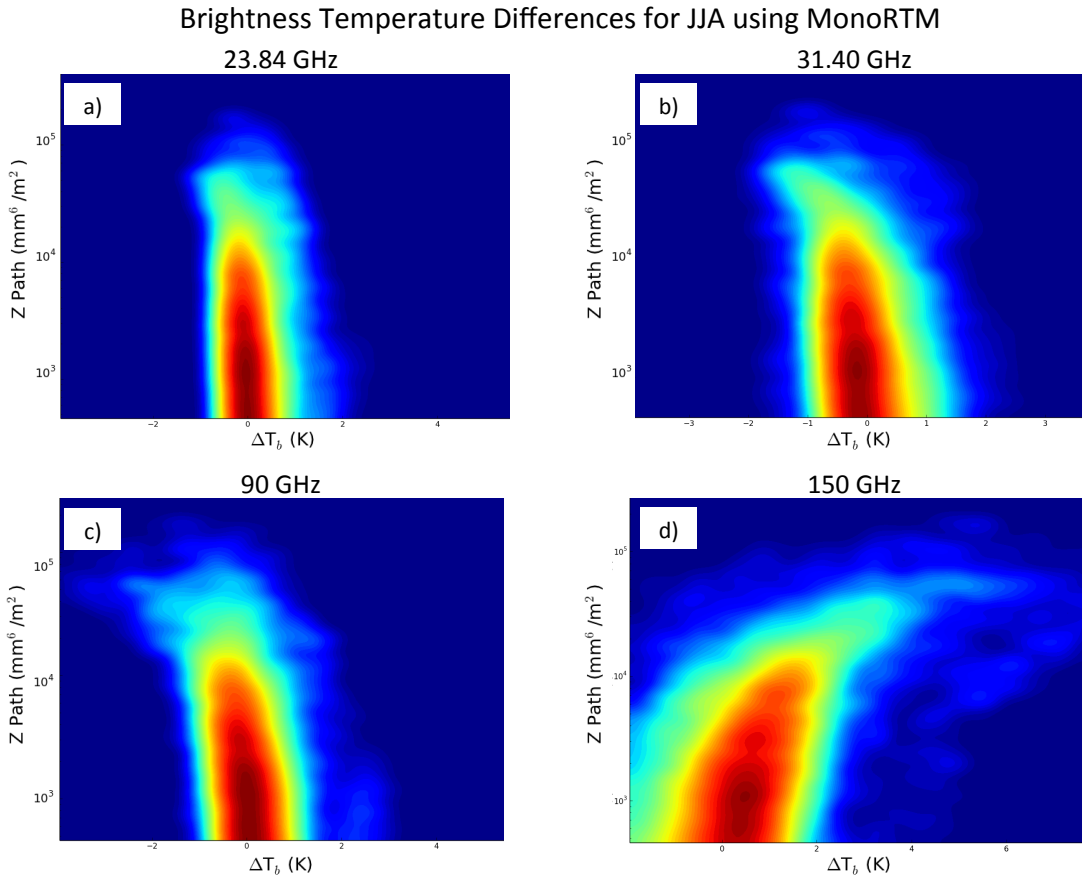

Figure 3.5: Brightness temperature differences between the observations from the MWR and MonoRTM for the 23.84, 31.40, 90, and 150GHz channels.

4. Liquid Water Path Retrieval Influenced by Ice

As seen in the previous section, the retrieved LWP values when ice is present are incorrect. The MWRRET algorithm uses four channels to calculate the LWP – including the 90 and 150 GHz channels. These high frequency channels observe elevated brightness temperatures when ice hydrometeors are in the atmospheric column, which lead to derived LWPs that are larger than what is actually present in the column. Therefore, the negative bias in the lower frequencies is caused by an overestimation of the retrieved LWP causing the simulations at the lower frequencies to be unrealistically warm. Thus, a correction for the LWP as a function of the MMCR derived Z Path must be developed to accurately measure the ice signature.

4.1 Ice Signature Influence on Retrieved Liquid Water

As illustrated in Figure 3.4 in the previous section, the difference between measured and modeled brightness temperatures as a function of integrated reflectivity, analogous to the amount of ice in the column, increases in the 150 GHz channel (see Figure 3.4d). However, in the other three microwave channels examined, 28.34, 31.40, and 90 GHz, there is the opposite effect (Figures 3.4a, 3.4b, and 3.4c, respectively). This effect is an artifact in the simulated brightness temperatures caused by the following chain of events:

1. The presence of ice increases the observed brightness temperatures at 90 and 150 GHz but has little effect on the lower frequencies.
2. Since the LWP retrieval does not include the effects of ice, it accounts for this increase by increasing the retrieved LWP thus producing an LWP estimate biased high.

3. The spectral slope of liquid water absorption does however not match the spectral slope of the ice signature.
4. Thus when the retrieved LWP is used in our forward simulation (see Figure 4.1a) it will produce brightness temperatures that are too high at the lower frequencies (in this case, 23.84, 31.40 and 90 GHz) and too low at the higher frequencies (150 GHz).

To better illustrate this idea it is useful to look at a modified version of Figure 2 from Kneifel *et al.* (2010), where the optical thickness as a function of frequency is plotted for several absorption models – for example, water vapor, liquid water, ice by habit, etc. (see Figure 4.1a). The frequency channels we examined in the previous section are highlighted with red arrows (23.84, 31.40, 90, and 150 GHz). Seen in Figure 4.1a, the liquid water and ice optical depths are less than 0.2 for these frequencies, so the brightness temperatures are approximately a linear combination of each component. Because of the approximately linear relationship between optical depth and brightness temperature, a schematic figure can be drawn in terms of brightness temperature rather than optical depth, keeping the relative spectral slopes in the 90 – 150 GHz region shown in the modified Kneifel figure. This schematic is shown in Figure 4.1b, with an Observed Spectrum (including ice signature), Spectrum with Retrieved LWP (no ice signature), and a theoretical Spectrum with "True" LWP (no ice signature) as a function of brightness temperature with respect to frequency.

As schematically illustrated in Figure 4.1b, the Observed Spectrum brightness temperatures compared to the Spectrum with Retrieved LWP are higher at 150 GHz but lower at 90 GHz. When the same comparison is made with the Spectrum with "True" LWP, which does not include the effect of the ice, both the 90 and 150 GHz observed brightness

temperatures are higher. The Spectrum with "True" LWP, illustrated in Figure 4.1b, is below both the measure values at 90 and 150 GHz and would yield the enhanced brightness temperature difference we expect. So, if the LWP can be corrected in the presence of ice, there should be enhanced brightness temperatures at the high frequency and no dependence at the low frequency channels. Because the liquid absorption model uses the MWR retrieved LWP as an input to the SOI, a correction for liquid water retrieved in the presence of ice is necessary to accurately quantify the ice.

4.2 Ice Influenced Liquid Water Path Correction

In Section 3, the observations of the differences in brightness temperatures measured and modeled showed a positive dependence on integrated reflectivity for the 150 GHz channel, but negative dependency for the other three channels. Since we know the lower frequency channels are comparably insensitive to ice, we can focus on the 31.40 GHz to derive a correction for the LWP – 23.84 GHz is in a water vapor absorption line and thus not a good candidate for the correction, whereas the 31.40 GHz is essentially a window channel. In the 31.40 GHz channel, we use the relationships of the change in the forward model as a function of change in LWP, and the change in the Z Path as a function of the change in brightness temperature together to derive a simple linear correction for the LWP when ice is present.

To correct the LWP in the presence of ice, a constant that describes the change in retrieved LWP as a function of the change in Z Path must be derived (ΔLWP/ΔZ Path). This can be achieved by finding the derivative of the forward model, ΔF, with respect to LWP, and combining it with the change in brightness temperature as a change in Z Path determined

by the contour plot. Both relationships appear to be quite linear. In Figure 4.2a, the forward model derivative was estimated with a finite difference method, by perturbing the LWP by 5 g/m^2. The change in radiance is approximately 0.38 K, with about +/- 5% scatter and no strong slope with respect to LWP. This indicates the forward model is approximately linear in LWP, yielding a constant, *A*:

$$A = \frac{\Delta F}{\Delta LWP}$$

where the above ΔF is the difference in brightness temperatures (K). In Figure 4.2b, the dashed line shows trace of the peaks in the histogram at each Z path value. This too shows an approximately linear function of Z path in the 31.40 GHz channel, which yields the second constant, *B*:

$$B = \frac{\Delta T_b}{\Delta Z\ Path}$$

If we then combine these two constants, we have a our LWP as a function of ice relationship needed for the correction:

$$C = \frac{B}{A} = \frac{\frac{\Delta T_b}{\Delta Z\ Path}}{\frac{\Delta F}{\Delta LWP}} = \frac{\Delta LWP}{\Delta Z\ Path}$$

Based on the observations and radiative transfer model runs in the 31.40 GHz channel, we calculated a value *C*:

$$C = -3.33 * 10^{-4} \frac{g/m^2}{mm^6/m^2} \pm \sim 3 * 10^{-5} \frac{g/m^2}{mm^6/m^2}$$

This constant can be combined with the co-located reflectivity measurements from the MMCR to correct for the effect of the ice on the LWP.

We now include the integrated reflectivity from the MMCR when constructing our radiative transfer model for a given day. The MMCR Z Path is combined with the above constant, *C*, and added to the MWRRET derived LWP to retrieve a corrected value. Comparison of the MWR observed data with the radiative transfer model – using the corrected LWP for ice – for the JJA season from 2011 through 2013 for LWP of less than 40 g/m^2 in the 31.40 GHz channel is now insensitive with respect to the integrated reflectivity (see Figure 4.3). The correction is successful in removing the extra LWP, as the 31.40 GHz channel comparison shows no influence from ice. Now that there is a successful correction for the ice influenced LWP, we can rerun the model on the other channels and characterize the signature from the ice hydrometeors.

4.3 Figures

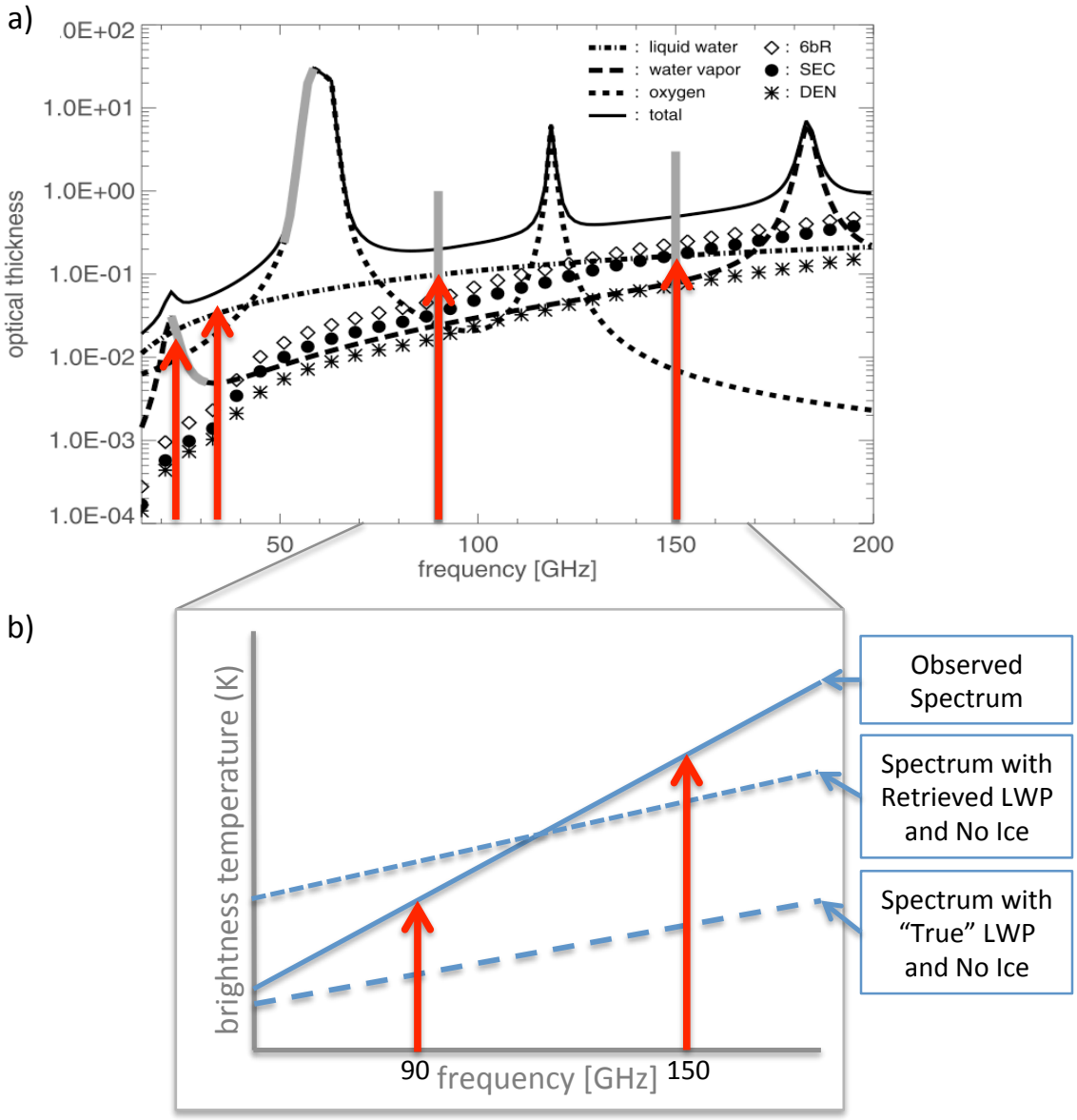

Figure 4.1: Kneifel *et al.* (2010), Figure 2 modeled output optical depth as a function of frequency with red arrows to highlight the microwave channels used in the LWP retrieval (part a). Panel b) is a zoomed schematic of the 90 and 150 GHz channels with brightness temperature (analogous for this case as discussed in the main text) as a function of frequency. The point of the schematic is to exaggerate the different effects of the MWR observed values when compared to the two different liquid water cases.

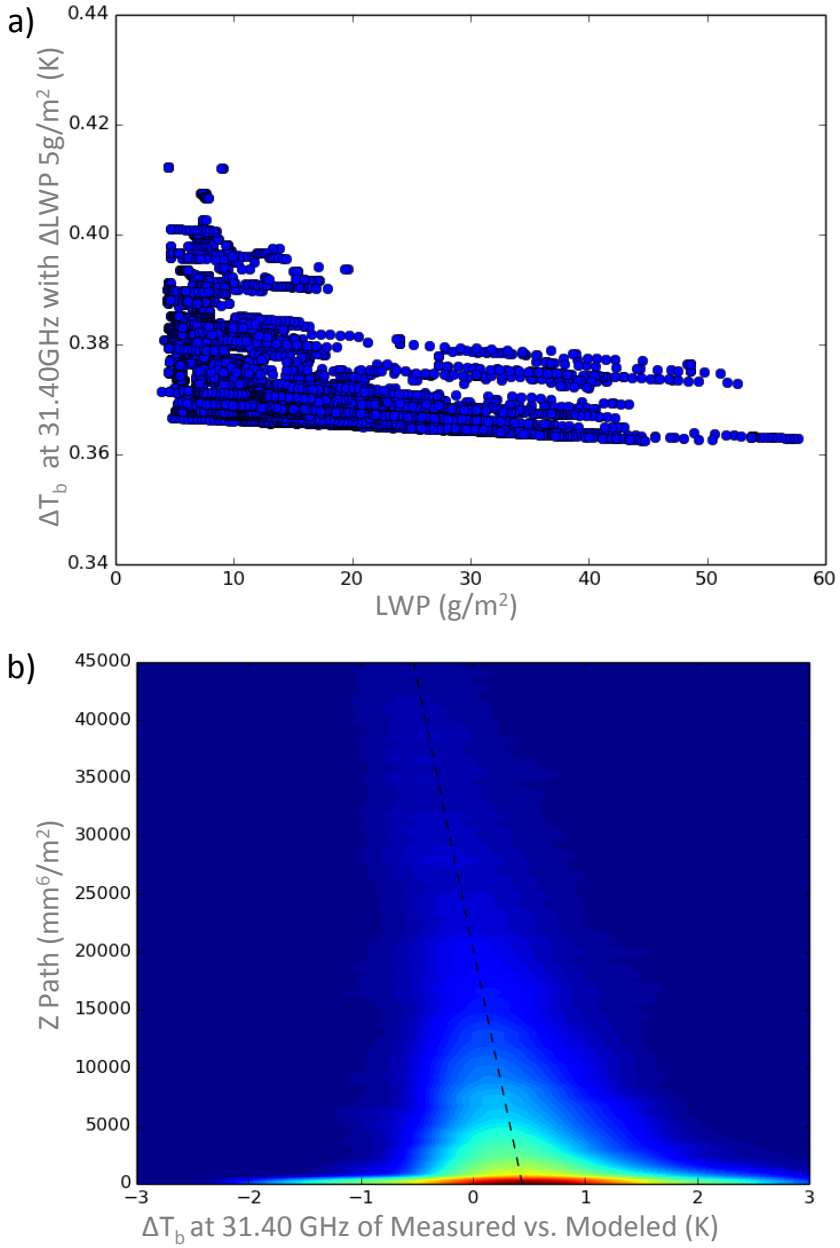

Figure 4.2: To calculate the constant LWP as a function of ice as measured by the MMCR, first a relationship between the forward model output and a defined LWP is needed. Panel a) shows the change in the brightness temperature between the original LWP and +5 g/m^2 as a function of the LWP originally in the column in the 31.40 GHz channel. There is essentially a linear relationship, with ~5% spread in brightness temperature, that yields a $\Delta F/\Delta LWP$ relationship. In Panel b) of the figure, the contour plot of the MMCR retrieved Z Path and the difference between the measured and modeled brightness temperature at 31.40 GHz has a roughly linear relationship applied to the peak values. This relationship yields the relationship of $\Delta T_b/\Delta Z$ Path. By combining these relationships, the change in LWP as a function of ice is calculated.

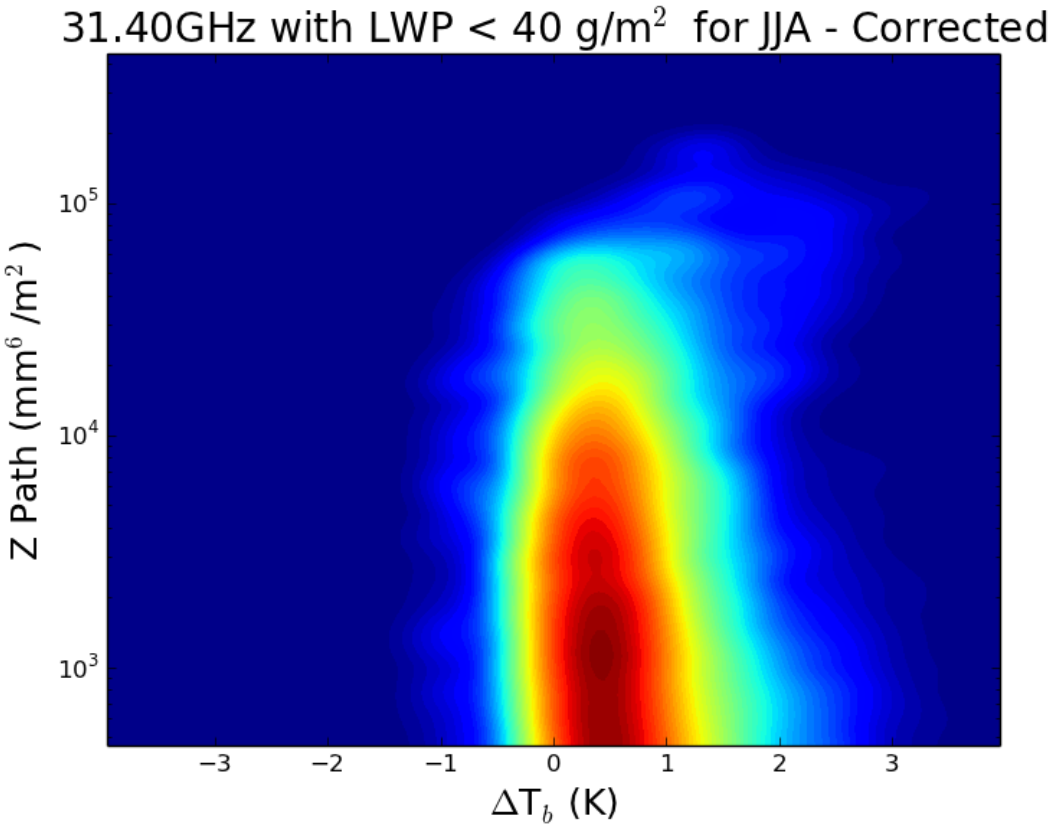

Figure 4.3: Brightness temperature differences between the observations from the MWR and the radiative transfer model for the 31.40 GHz channel with the corrected LWP in the presence of ice.

5. Brightness Temperatures Differences as Measureable Ice Signature

5.1 Brightness Temperature Differences with Corrected LWP

We again focus on cases in JJA with LWP of less than 40 g/m^2, not including the clear sky. These cases represent the majority of times at Summit during the summer months when there is the maximum amount of ice precipitation. Similar to the figures shown in subsections 3.2 and 3.3, the measured MWR observations are compared with the radiative transfer model with the added LWP correction for ice, outlined in section 4.3. Similar contour plots are produced for the summer season (2011 through 2013) at Summit for the same four channels: 23.84, 31.40, 90, and 150 GHz. The results for the lower frequency channels, shown in Figure 5.1a and b, now have no dependency on the Z Path – as expected. In the high frequency channels, 90 and 150 GHz, there is clearer relationship of the positive dependence of the brightness temperature difference on Z Path from the MMCR – thus, indicative of ice enhanced brightness temperatures.

5.2 Comparison of Ice Signatures Observed with Scattering Model Results

To associate the ice signature we have now identified in the high frequency MWR channels for JJA at Summit to a specific ice habit, it is necessary to convert the MMCR reflectivity to layer optical properties for input to the SOI model. To do this, we first need a scattering model for the ice crystal shape and a particle size distribution (PSD). We can find the difference in modeled brightness temperatures in the presence of ice using SOI by running the model twice, once including ice and once with only gas and liquid water. By comparing these modeled differences to those found in our measurement derived

comparisons from ICECAPS data, we may be able to say something more specific with regard to ice habit or particle size distribution.

For an initial ice habit study, we used the temperature-dependent Field *et al.* (2007), databases for the particle size distribution, which are a result of a flight campaign of in-situ measurements of stratiform ice clouds in the midlatitudes. Additionally, we used information from the Liu database of microwave single-scattering properties for three-bullet rosettes (LR3), sectored snowflakes (LSS), and dendrites (LDS) for ice habit characteristics (see Figure 5.2; Liu *et al.*, 2008). The PSD and ice habit information is used to convert the measurements by the MMCR from reflectivity to an ice water content (IWC), which is then used to calculate optical properties of the column. These optical properties are fed into the SOI model to calculate a brightness temperature at designated frequencies. Finally, the emissivity of the snow surface is accounted for using data from Yan *et al.* (2008) based on conditions at Summit Station and the microwave frequency of the brightness temperature output (see Table 5.1).

By running the SOI model twice, once including ice and once with only gas and liquid water, we calculated a difference in brightness temperature as a function of frequency analogous to the difference in brightness temperature of the measured and modeled results shown in Figure 5.1. For these SOI model runs, we used a surface emissivity of 0.6 (the difference of 0.6 versus 0.9 surface emissivity results in less than 1 K difference for both the 90 and 150 GHz channels) and ice habits LR3, LSS, and LDS as these are the same as those used in the Kneifel *et al.* (2010) case study. We can gain insight into the habits and PSDs at Summit by comparing these brightness temperature differences in the 90 and 150 GHz

derived from the SOI for several different ice habits against the results from the measurements.

To compare the modeled and measured results, it is first useful to plot the relationship of the difference in the brightness temperatures at the 90 and 150 GHz as a function of each other. Figure 5.3 depicts the observed ice signature at 150 GHz versus the same at 90 GHz and there is a distinct linear relationship between the ice effects at the two frequencies (approximated with black, dashed line). Also important to note is that the enhancement of the brightness temperature from the ice is almost double the effect at 150 GHz as compared to 90 GHz. All the SOI model results show a much higher slope in the relationship of brightness temperature difference in the 150 GHz as a function of that in the 90 GHz channel versus the same relationship seen from the MWRHF observations.

Clearly there are some major differences between the SOI model results and the observations, likely stemming from the ice habit assumptions and/or the PSD used for these initial results. First of all, we can run SOI for only a single habit at a time and the model runs for these habits should bound the observations if assumptions made from the PSD are correct. Since the three habits we ran are so different from the measurements, this leads us to believe the Field *et al.* (2007) parameterization may not adequately represent PSDs in Arctic environments. The Field *et al.* (2007) parameterization is derived from midlatitude flight campaign measurements of ice stratiform clouds and may very well be not at all applicable to the arctic (Field *et al.*, 2005; 2007). Additionally, the Field, *et al.* (2007), parameterization assumes aggregated ice particles, while non-aggregated, pristine ice crystals are commonly observed at Summit (see Figure 5.4). Furthermore, the temperatures observed in the Field *et al.* (2007) parameterization are much higher than those at Summit, as it is located in and

around the United Kingdom, and therefore the growth mechanisms of the ice hydrometeors in this PSD may be much different than those in the Arctic. From our observations of the ice signature compared to the model output differences in brightness temperature, we believe that the Field *et al.* (2007), PSD may not be applicable to the conditions at Summit. Further work will explore other PSDs and particle size relationships, which will aid our understanding of the ice habits at Summit.

5.3 Tables and Figures

Table 4. Ten Microwave Snow Emissivity Spectra Used in Generating the Simulated Satellite Brightness Temperatures[a]

Snow Type	23.8 GHz	31.4 GHz	50.3 GHz	89 GHz	150 GHz
Fresh snow	0.94	0.94	0.93	0.92	0.90
Grass after snow	0.91	0.90	0.90	0.91	0.86
RS snow (A)	0.86	0.86	0.85	0.82	0.82
RS snow (C)	0.84	0.83	0.82	0.79	0.73
RS snow (E)	0.78	0.77	0.76	0.72	0.72
Thin crust snow	0.95	0.93	0.87	0.74	0.65
Bottom crust snow (A)	0.76	0.75	0.75	0.70	0.69
Deep snow	0.81	0.77	0.74	0.69	0.64
Bottom crust snow (B)	0.84	0.76	0.66	0.48	0.44
Thick crust snow	0.86	0.74	0.63	0.50	0.45

a *Yan et al.* [2004]. RS stands for radiometric snow that implies a distinct emissivity spectrum but cannot be directly associated with a physical snow type.

Table 5.1: Surface emissivity for different snow conditions in the microwave channels of 23.8, 31.4, 50.3, 90, and 150GHz channels. For our study at Summit Station, the applicable snow types assumed were Fresh snow, Thin crust snow, and Deep snow. The GIS at Summit rarely melts, so there would rarely be a thick crust or bottom crust, and the snow/ice pack is 3000+ meters thick, so there is no grass or dirt under or over snow to consider (*Table 4 from Yan, 2008*).

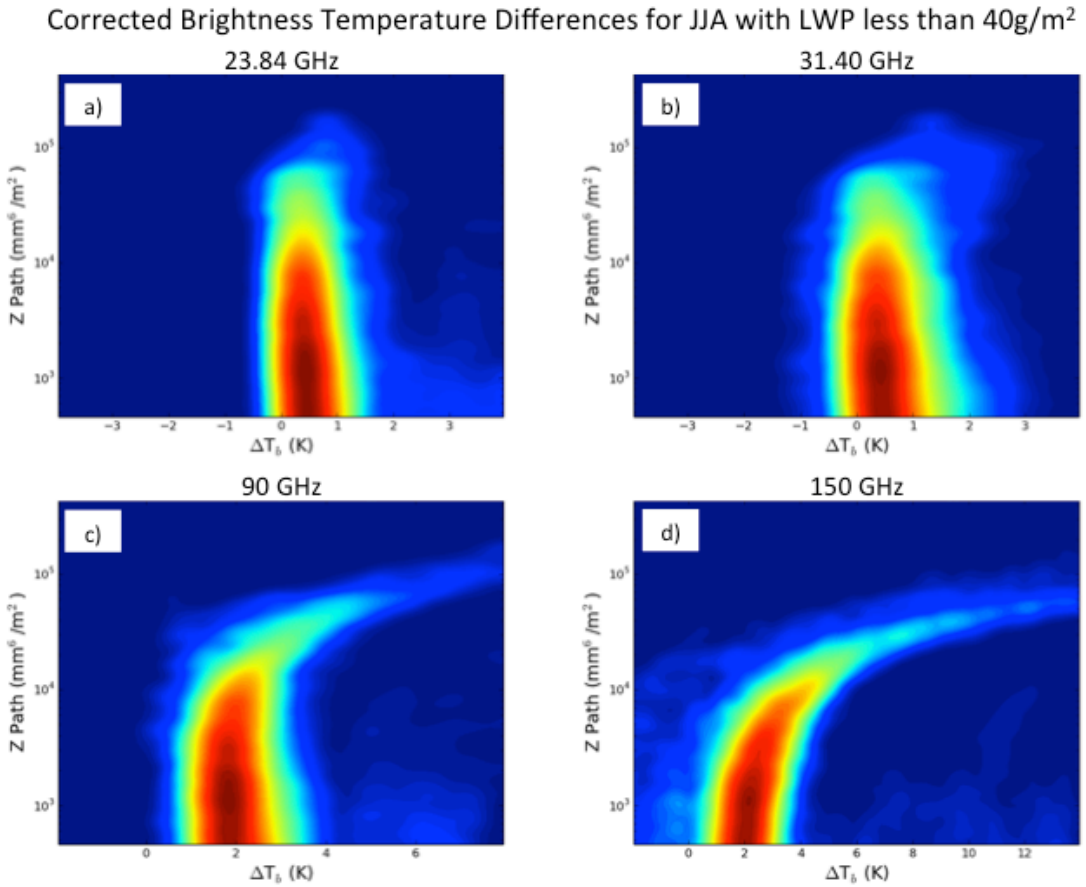

Figure 5.1: Brightness temperature differences between the observations from the MWR and the radiative transfer with the LWP correction for ice for the 23.84, 31.40, 90, and 150GHz channels with the corrected LWP values. There is now no dependence of the brightness temperature difference in the lower frequency channels (a and b), as would be expected since they are insensitive to ice in the column. The high frequency channels (c and d) show a clear dependence of the difference in brightness temperature and the Z Path from the MMCR – thus, indicating an increasing brightness temperature in these channels with increasing total ice amount in the column.

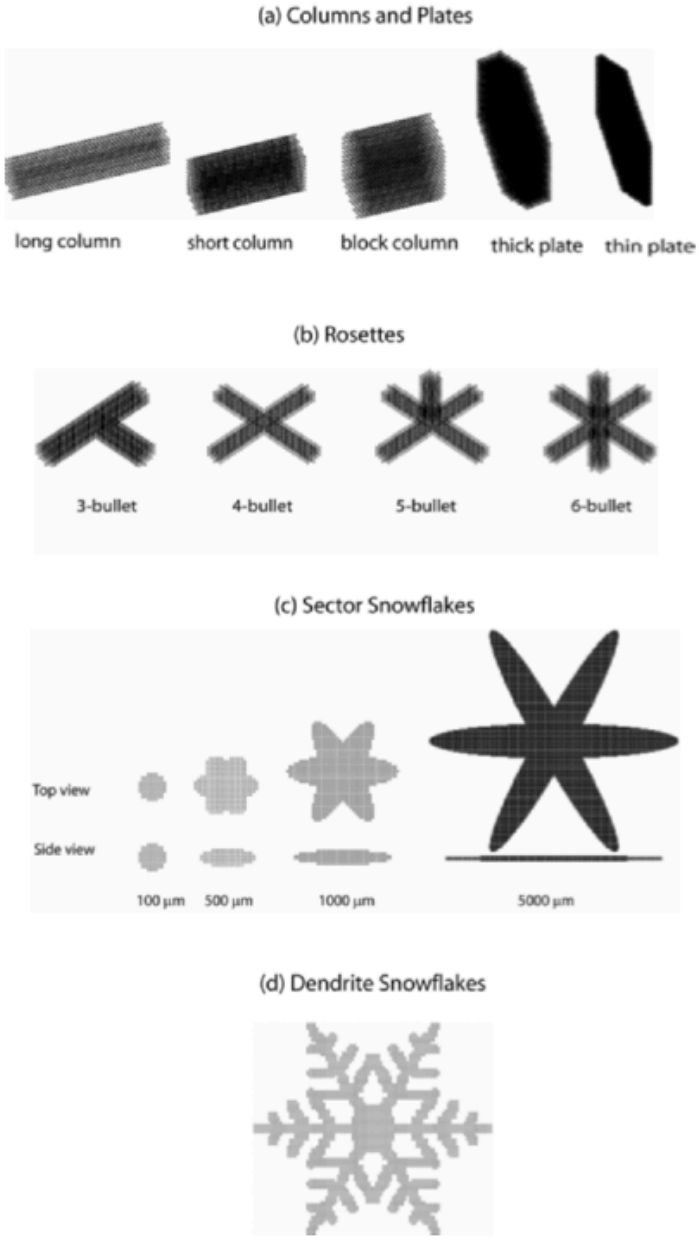

Figure 5.2: Shapes of hydrometeors available from the Liu database of microwave properties of nonspherical ice. Panel a) shows column and plates, Panel b) shows rosettes, Panel c) illustrates various sector snowflakes, and Panel d) is a dendrite. For this study, three-bullet rosette (LR3), sector snowflake (LSS), dendrite (LDS) ice habits were used (*Figure 1 from Liu, 2008*).

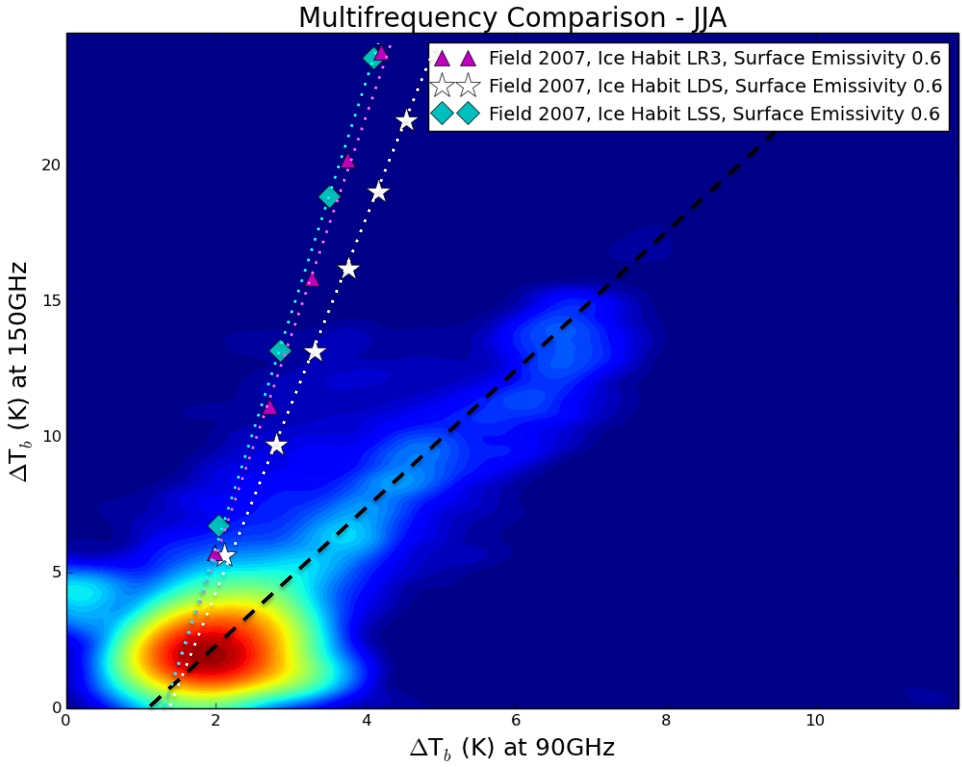

Figure 5.3: Brightness temperature differences between the observations from the MWR and the radiative transfer with the LWP correction for ice for the 90GHz vs. the 150GHz channel with the SOI model run results superimposed. The model was run for the LR3, LDS, and LSS ice habits, using the Field *et al.* (2007) PSD, with an assumed surface emissivity of 0.6 (at the low end of the range for snow as determined by Yan *et al.*, 2008). It is clear that the SOI model results using these assumed parameters are not valid with respect to the measured ice hydrometeor signature we see at Summit.

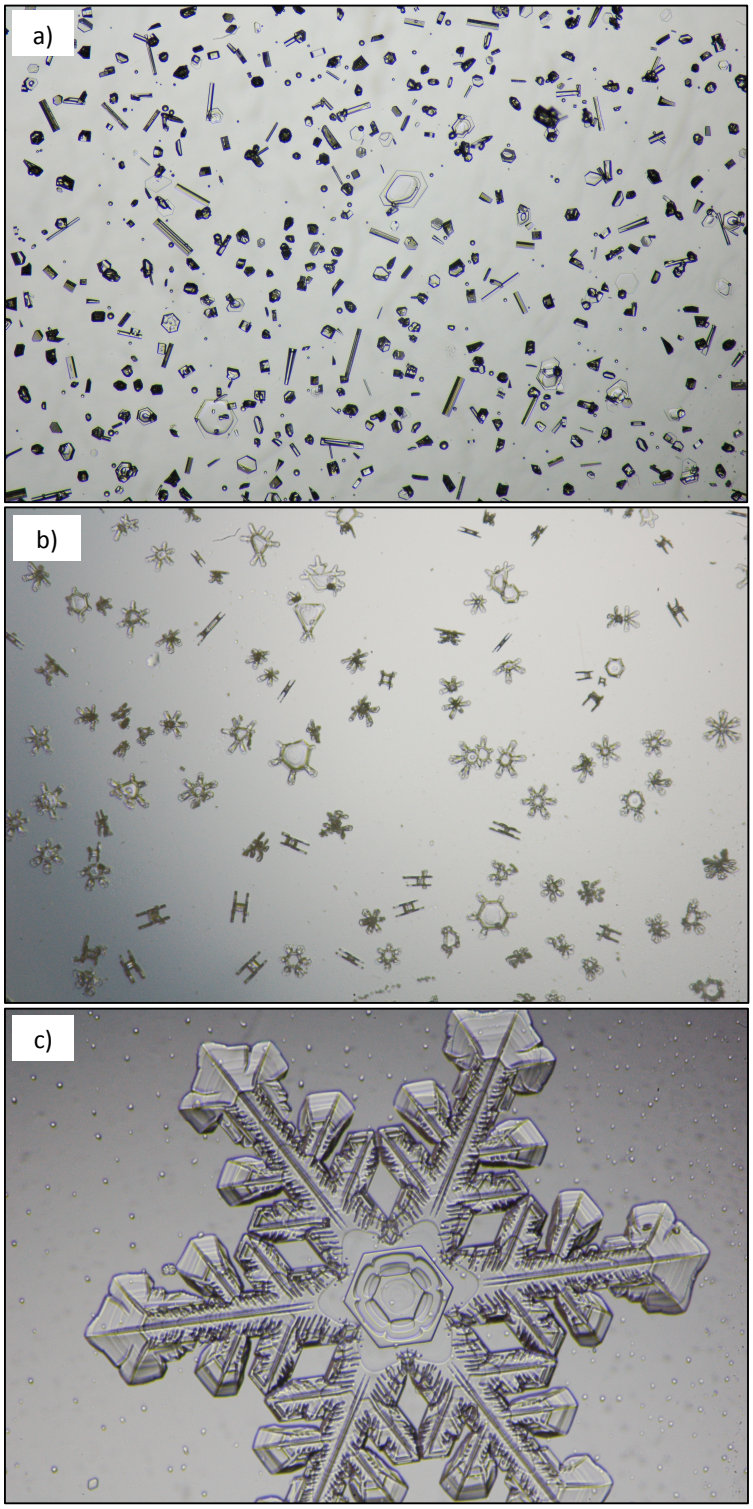

Figure 5.4: IcePIC instrument pictures of crystals sampled from different days at Summit Station. There are many different ice habits that occur in a given sampling as illustrated in part a. Additionally, pristine forms of ice habits are a common – for example, capped columns in part b and the dendrite in part c.

6. Conclusions

This work suggests several directions to improve understanding of high frequency microwave signatures of ice hydrometeors. First, though we provided a simple solution to correct the ice influenced LWP retrieval in section four; a more formal correction should be implemented within the LWP retrieval. It may be possible to combine the MWRRET algorithm with data from the MMCR to create a robust retrieval of the LWP when ice is present in the column. It is important to have high accuracy in the LWP values as that corresponds directly to the quantification of the ice hydrometeor signature seen in the MWRHF channels. Once a formal retrieval is in place for the ice influenced LWP values, we can then test many different PSDs and ice habits against the measured ice signature and validate those that are applicable to the conditions at Summit.

Additionally, as discussed in the previous section, the ice behavior is very difficult to model and we are certainly not yet able to reproduce similar enhanced brightness temperatures as those seen in the HFMWR channels. To accurately model the ice signature, we need accurate descriptions of the ice habit, surface emissivity, and a PSD representative of conditions at Summit. Since we see large differences in the measured ice signature at Summit and the modeled brightness temperatures, we can therefore conclude that the combination of Field *et al.* (2007) PSD and ice habit models used in this study are likely not appropriate for the unique conditions observed above the GIS. For future work, we hope to employ a PSD with a better fit to the Summit conditions and eventually have ICECAPS instrumentation capable of measuring a PSD *in-situ*. Currently, the IcePIC images lend some

insight to ice hydrometeor characteristics at Summit, but more information is needed to produce accurate models of the ice signature.

Further, since thin liquid cloud conditions occur often in the Arctic, one cannot neglect the influence of ice in the LWP retrievals. The technique illustrated in this paper can be used at other ground sites with similar instrument capabilities (i.e., Barrow, SHEBA, Finland) during times when the temperatures are consistently below freezing to characterize ice signature and correct the retrieved LWP. The measured ice signature technique outlined in this work is a novel approach to better understand ice hydrometeors and could prove to be a powerful tool in future ground and remote sensing applications.

Appendix A: Acronyms

Acronym	Name
ARM	Atmospheric Radiation Measurement Program
CBH	Cloud Base Height
CFAD	Contoured Frequency by Altitude Diagram
GIS	Greenland Ice Sheet
HATPRO	Humidity and Temperature PROfiler
ICECAPS	Integrated Characterization of Energy, Clouds, Atmospheric State and Precipitation at Summit
IcePIC	Ice Particle Imaging Camera
IWC	Ice Water Content
IWP	Ice Water Path
JJA	June, July, August
LDS	Liu Dendrite Snowflake
LR3	Liu Three-Bullet Rosette
LSS	Liu Sector Snowflake
LWC	Liquid Water Content
LWP	Liquid Water Path
MMCR	Millimeter Cloud Radar
MonoRTM	Monochromatic Radiative Transfer Model
MWR	Microwave Radiometer
MWRHF	Microwave Radiometer High Frequency
PSD	Particle Size Distribution
PWV	Precipitable Water Vapor
RT	Radiative Transfer
RH	Relative Humidity
SOI	Successive Order of Interaction
SSA	Single Scatter Albedo
US AON	United States Arctic Observation Network
UTC	Coordinated Universal Time

REFERENCES

Ackerman, T. & G. Stokes (2003). The Atmospheric Radiation Measurement Program. *Physics Today, 55*, 39-44

Bailey, M. & J. Hallett (2009). A Comprehensive Habit Diagram for Atmospheric Ice Crystals: Confirmation from the Laboratory, AIRS II, and Other Field Studies. *Journal of Atmospheric Science, 66*, 2888-2899.

Bennartz R. & G. Petty (2001). The Sensitivity of Microwave Remote Sensing Observations of Precipitation to Ice Particle Size Distributions. *Journal of Applied Meteorology, 40*, 345-364.

Bennartz, R. & P. Bauer (2003). Sensitivity of microwave radiances at 85–183 GHz to precipitating ice particles. *Radio Science, 38*(4), 8075, doi:10.1029/2002RS002626

Church, J. (2001). Changes in sea level. *Climate Change 2001: The Scientific Basis,* J. T. Houghton et al., Eds., Cambridge University Press, 639–693.

Crewell, S., and U. Löhnert (2003). Accuracy of cloud liquid water path from ground-based microwave radiometry 2. Sensor accuracy and synergy. *Radio Science, 38*(3), 8042-8051. doi:10.1029/2002RS002634

Crewell, S., and U. Löhnert (2007). Accuracy of boundary layer temperature profiles retrieved with multifrequency multiangle microwave radiometry. *IEEE Transactions on Geoscience and Remote Sensing, 45*, 2195-2201.

Crewell, S., K. Ebell, U. Löhnert, & D. D. Turner (2009). Can liquid water profiles be retrieved from passive microwave zenith observations? *Geophysical Research Letters, 36*, L06803. doi:10.1029/2008GL036934

Dansgaard, W., S. Johnsen, H. Clausen, D. Dahl-Jensen, N. Gundestrup, C. Hammer, C. Hvldberg, J. Steffensen, A. Sveinbjörnsdottir, J. Jouzel, & G. Bond (1993). Evidence for general instability of past climate from a 250-kyr ice-cor record. *Nature, 364*, 218-220.

Field, P., R. Hogan, P. Brown, A. Illingworth, T. Choularton, & R. Cotton (2005). Parameterization of ice-particle size distributions for mid-latitude stratiform cloud. *Quarterly Journal of the Royal Meteorolgical Society, 131*, 1997-2017, doi:10.1256/qj.04.134

Field, P., A. Heymsfield, & A. Bansmer (2007). Snow Size Distribution Parameterization for Midlatitude and Tropical Ice Clouds. *Journal of the Atmospheric Sciences, 64*, 4346-4365.

Heidinger, A., C. O'Dell, R. Bennartz, & T. Greenwald (2006). The Successive-Order-of-Interaction Radiative Transfer Model. Part I: Model Development. *Journal of Applied Meteorology and Climatology, 45*, 1388-1402.

Hong G., G. Heygster, J. Miao, & K. Kunzi (2005). Detection of tropical deep convective clouds from AMSU-B water vapor channels measurements. *Journal of Geophysical Research, 110*, D05205, doi:10.1029/2004JD004949

Kneifel, S., U. Löhnert, A. Battaglia, S. Crewell, and D. Siebler (2010). Snow scattering signals in ground based passive microwave radiometer measurements. *Journal of Geophysical Research, 115*, D16214, doi:10.1029/2010JD013856

Kneifel, S., R. Bennartz, & M. Kulie (2011). A triple-frequency approach to retrieve microphysical snowfall parameters. *Journal of Geophysical Research, 116*, D11203, doi:10.1029/2010JD015430

Kulie, M. & R. Bennartz (2009). Utilizing space-borne radars to retrieve dry snowfall. *Journal of Applied Meteorology and Climatology, 48,* 2564–2580, doi:10.1175/2009JAMC2193.1

Kulie, M., R. Bennartz, T. Greenwald, Y. Chen, & F. Weng (2010). Uncertainties in Microwave Properties of Frozen Precipitation: Implications for Remote Sensing and Data Assimilation. *Journal of Atmospheric Science, 67*, 3471-3487.

Liebe, H., G. Hufford, & T. Manabe (1991). A model for the per-mittivity of water at frequencies below 1THz, Internat. *Jounral of Infrared Millimeter and Terahertz Waves, 12*, 659-675.

Liu, G. (2008). A database of microwave single-scattering properties for nonspherical ice particles. *Bulletin of the American Meteorological Society, 89*, 1563-1570, doi:10.1175/2008BAMS2486.1

Löhnert, U., S. Crewell, A. Macke, & C. Simmer (2001), Profiling cloud liquid water by combining active and passive microwave measurements with cloud model statistics. *Journal of Atmpspheric and Oceaniac Technology, 18*, 1354-1366.

Löhnert, U., and S. Crewell (2003). Accuracy of cloud liquid water path from ground-based microwave radiometry, 1, Dependency on cloud model statistics. *Radio Science, 38*(3), 8041, doi:10.1029/2002RS002654

Moran, K., B. Martner, M. Post, R. Kropfli, D. Welsh, & K. Widener (1998). An unattended cloud-profiling radar for use in climate research. *Bulletin of the American Meteorological Soc*iety*, 79*, 443–455.

O'Dell, C., A. Heidinger, T. Greenwald, P. Bauer, and R. Bennartz (2006). The Successive-Order-of-Interaction Radiative Transfer Model. Part II: Model Performance and Applications. *Journal of Applied Meteorology and Climatology, 45*, 1403-1413.

Petty, G. & W. Huang (2010), Microwave backscatter and extinction by soft ice spheres and complex snow aggregates. *Journal of Atmospheric Science, 67*, 769-787, doi:10.1175/2009JAS3146.1

Pruppacher, H. & Klett, J. (2000) *Microphysics of clouds and precipitation* (2nd Ed.). The Netherlands: Kluwer Academic Publishers.

Rinehart, R. (2010). *Radar for Meteorologists* (5th Ed.). Nevada, Missouri: Rinehart Publications.

Rose, T., S. Crewell, U. Löhnert, & C. Simmer (2005). A network suitable microwave radiometer for operational monitoring of the cloudy atmosphere. *Atmospheric Research, 75*, 183-200, doi:10.1016/j.atmosres.2004.12.005

Rosenkranz, P. (1998). Water vapour microwave continuum absorption: A comparison of measurements and models. *Radio Science, 33*, 919-928, doi:10.1029/98RS01182

Shupe, M., T. Uttal, & S. Matrosov (2005). Arctic cloud microphysics retrievals from surface-based remote sensors at SHEBA. *Journal of Applied Meteorology, 44*, 1544-1562.

Shupe. M., T. Uttal, & S. Matrosov (2006). Arctic mixed- phase cloud properties derived from surface-based sensors at SHEBA. *Journal of Atmospheric Science, 63*, 697-711.

Shupe, M. (2007). A ground-based multisensor cloud phase classifier. *Geophysical Review Letters, 34*, L22809, doi:10.1029/2007GL031008

Shupe, M., V. Walden, E. Eloranta, T. Uttal, J. Campbell, S. Starkweather, & M. Shiobara (2011). Clouds at Arctic atmospheric observatories, Part I. Occurrence and macrophysical properties. *Journal of Applied Meteorology and Climatology, 50*, 626-644.

Shupe, M., D. Turner, V. Walden, R. Bennartz, M. Cadeddu, B. Castellani, C. Cox, D. Hudak, M. Kulie, N. Miller, R. Neely, W. Neff, & P. Rowe (2013). High and Dry: New Observations of Tropospheric and Cloud Properties above the Greenland Ice Sheet. *Bulletin of the American Meteorological Society, 94*(2), 169-186.

Skofronick-Jackson, G., J. Wang, G. Heymsfield, R. Hood, W. Manning, R. Meneghini, & J. Weinman (2002). Combined Radiometer–Radar Microphysical Profile Estimations with Emphasis on High-Frequency Brightness Temperature Observations. *Journal of Applied Meteorology, 42*, 476-486.

Turner, D., S. Clough, J. Liljegren, E. Clothiaux, K. Cady-Pereira, & K. Gaustad (2007). Retrieving Liquid Water Path and Precipitable Water Vapor From the Atmospheric Radiation Measurement (ARM) Microwave Radiometers. *IEEE Transactions on Geoscience and Remote Sensing, 45*(11), 3680-3690.

Turner, D., A. Vogelmann, R. Austin, J. Banard, K. Cady-Pereira, J. Chiu, S. Clough, C. Flynn, M. Khaiyer, J. Liljegren, K. Johnson, Q. Min, P. Minnis, W. O'Hirok, Z. Wang, & W. Wiscombe (2007a). Thin liquid water clouds: Their importance and our challenge. *Bulletin of the American Meteorological Society, 88*, 177-190.

Yan. B., F. Weng, & H. Meng (2008). Retrieval of snow surface microwave emissivity from the advanced microwave sounding unit. *Journal of Geophysical Research, 113*, D19206, doi:10.1029/2007JD009559